# Image Cover Sheet

| CLASSIFICATION | SYSTEM NUMBER | 150919 |
|---|---|---|
| UNCLASSIFIED | | |

**TITLE**

SABOT DESIGN, FREE-FLIGHHT TESTS AND ANALYSIS OF A TANDEM PROJECTILE
CONFIGURATION AT MACH 2

**System Number:**

**Patron Number:**

**Requester:**

**Notes:**

**DSIS Use only:**

**Deliver to:**      FF

## Report Documentation Page

| 1. REPORT DATE **FEB 1995** | 2. REPORT TYPE | 3. DATES COVERED |
|---|---|---|

| 4. TITLE AND SUBTITLE | 5a. CONTRACT NUMBER |
|---|---|
| **Sabot Design, Free-Flight Tests and Analysis of a Tandem Projectile Configuration at Mach 2** | 5b. GRANT NUMBER |
| | 5c. PROGRAM ELEMENT NUMBER |
| 6. AUTHOR(S) | 5d. PROJECT NUMBER |
| | 5e. TASK NUMBER |
| | 5f. WORK UNIT NUMBER |

| 7. PERFORMING ORGANIZATION NAME(S) AND ADDRESS(ES) **Defence R&D Canada - Valcartier,2459 Pie-XI Blvd North,Quebec (Quebec) G3J 1X5 Canada, ,** | 8. PERFORMING ORGANIZATION REPORT NUMBER |
|---|---|
| 9. SPONSORING/MONITORING AGENCY NAME(S) AND ADDRESS(ES) | 10. SPONSOR/MONITOR'S ACRONYM(S) |
| | 11. SPONSOR/MONITOR'S REPORT NUMBER(S) |

12. DISTRIBUTION/AVAILABILITY STATEMENT
**Approved for public release; distribution unlimited.**

13. SUPPLEMENTARY NOTES

14. ABSTRACT

**A series of free-flight tests were conducted at Mach 2 to verify a sabot design that was used to launch a tandem projectile configuration, of similar profile and size, from a 110 mm smooth bore. The projectiles consisted of a four-fin cone-cylinder model with a length-todiameter ratio l/d of 6. Four shots were fired, two at an open range to test the sabot functioning and model-sabot integrity at launch, and two in the DREV aeroballistic range to obtain detailed trajectories of the projectiles to study aerodynamic interference effects. The sabot separation process, the measured trajectories, including the separation aspects of the trailing projectile relative to the leading one, are analyzed and discussed. The stability of the models and their aerodynamic characteristic are compared relative to each other and with the results of a same configuration fired individually. Detailed flow photographs showing the complex shock wave structure and their interference on both models flying in close proximity are also given.**

15. SUBJECT TERMS

| 16. SECURITY CLASSIFICATION OF: | | | 17. LIMITATION OF ABSTRACT | 18. NUMBER OF PAGES **99** | 19a. NAME OF RESPONSIBLE PERSON |
|---|---|---|---|---|---|
| a. REPORT **unclassified** | b. ABSTRACT **unclassified** | c. THIS PAGE **unclassified** | | | |

Défense National
nationale Defence

**UNCLASSIFIED**

### DEFENCE RESEARCH ESTABLISHMENT
### CENTRE DE RECHERCHES POUR LA DÉFENSE
### VALCARTIER, QUÉBEC
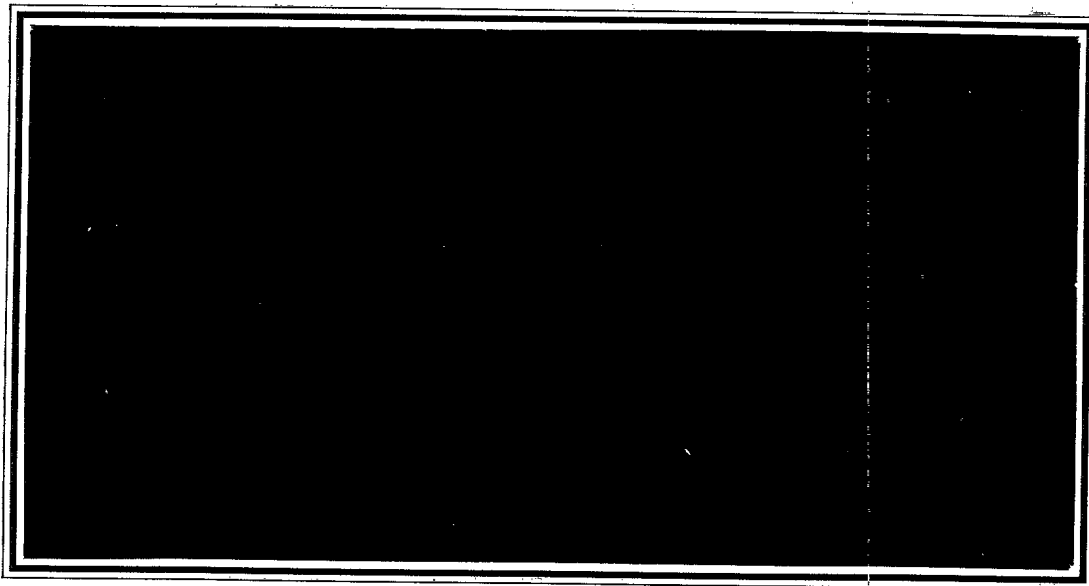
RESEARCH AND DEVELOPMENT BRANCH
DEPARTMENT OF NATIONAL DEFENCE
CANADA
BUREAU - RECHERCHE ET DÉVELOPPEMENT
MINISTÈRE DE LA DÉFENSE NATIONALE
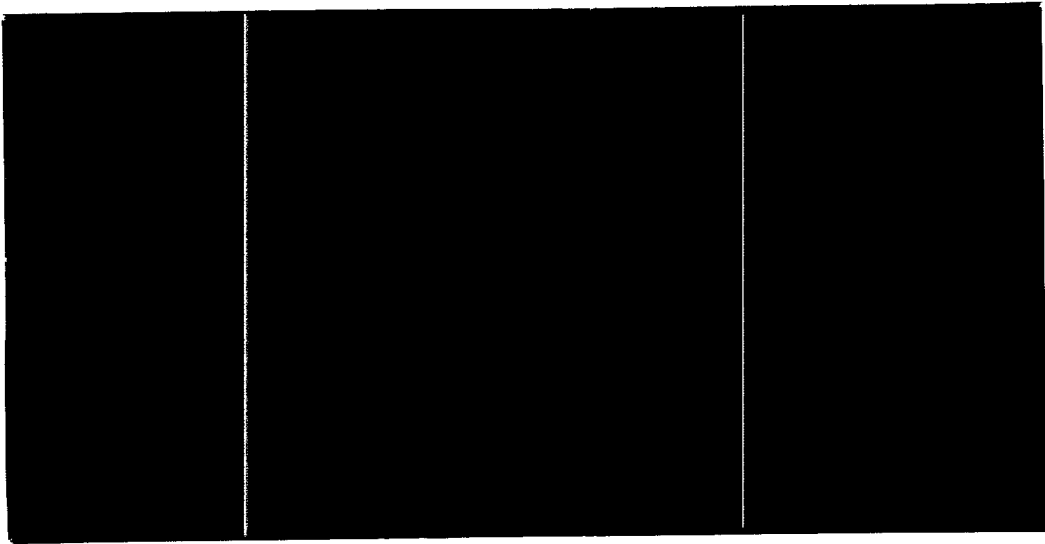
Canada

**SANS CLASSIFICATION**

UNCLASSIFIED

DEFENCE RESEARCH ESTABLISHMENT
CENTRE DE RECHERCHES POUR LA DÉFENSE
VALCARTIER, QUÉBEC

DREV - TM - 9441

SABOT DESIGN, FREE-FLIGHT TESTS AND ANALYSIS
OF A TANDEM PROJECTILE CONFIGURATION AT MACH 2

by

A. D. Dupuis and M. Normand

February/février 1995

Approved by / approuvé par

*[signature]*

Director / Directeur

*14 feb 95*

Date

SANS CLASSIFICATION

UNCLASSIFIED

i

ABSTRACT

A series of free-flight tests were conducted at Mach 2 to verify a sabot design that was used to launch a tandem projectile configuration from a 110 mm smooth bore gun and to obtain detailed trajectories of the projectiles to study aerodynamic interference effects. The projectiles were of similar profile and size and consisted of a four-fin cone-cylinder model with a length-to-diameter ratio (l/d) of 6. Four shots were fired, two at an open range to test the sabot functioning and model-sabot integrity at launch, and two in the DREV aeroballistic range. The sabot separation process, the measured trajectories, including the separation aspects of the trailing projectile relative to the leading one are analysed and discussed. The stability of the tandem models and their aerodynamic characteristic are compared relative to each other and with the results of a same configuration when fired individually. Detailed flow photographs showing the complex shock wave structure and their interference on both models flying in close proximity are also given.

RÉSUMÉ

Une série d'essais en vol libre ont été effectués à Mach 2 pour vérifier un concept de sabot qui a été conçu pour tirer des projectiles en configuration tandem d'un canon 110 mm à âme lisse et pour obtenir les trajectoires des projectiles pour étudier les effets d'interférence aérodynamique. Les projectiles étaient de profiles et grosseurs similaires et consistaient d'un modèle cone-cylindre à quatre ailettes avec un allongement (l/d) de 6. Quatre tirs ont été effectués, deux dans un champ de tirs pour tester le fonctionnent du sabot et l'intégrité du concept au lancement, et deux autres au corridor aérobalistique du CRDV. Le processus de la séparation du sabot, les trajectoires qui ont été mesurées, ainsi que les aspects de séparation entre le deuxième modèle relatif au premier, sont analysés et discutés. La stabilité des modèles tandems ainsi que les coefficients aérodynamiques sont comparés un par rapport à l'autre, et avec les résultats de la même configuration tirée individuellement. Des photos détaillées d'écoulement démontrant des ondes de chocs de structure complexe et leurs interférences sur les modèles volant en proximité sont aussi données.

UNCLASSIFIED
iii

## TABLE  OF  CONTENTS

UNCLASSIFIED

iv

UNCLASSIFIED

v

# EXECUTIVE SUMMARY

The advances in armour technology in the last decade and the ones being looked at for the future pose a challenging problem for the ammunition designer. Reactive armour, usually added on or appliqué, are in use today to defeat many high length-to-diameter ratio kinetic energy projectiles. Studies are being conducted on active armour for future tanks to defeat or diminish the effectiveness of existing anti-tank killers which consists mainly of APFSDS projectiles. One of the possible weapon systems that could be used to defeat an active armour defense system would be one that could fire projectiles in a tandem configuration at the target, from the same gun. The leading projectile would activate the defense mechanism and the trailing projectile would follow through to defeat the main armour. In all possibility, the trailing projectile would be guided in by the leading projectile.

Many studies have been conducted on the role of segmented projectiles and tandem projectiles on the terminal ballistics aspects. The information on how such tandem projectiles could be launched or fly in formation to the target is rather limited. The flight dynamic and aerodynamic aspects, such as interference effects of one projectile on the other, dispersion, stability and aerodynamic characteristic of such projectiles flying in a tandem configuration have to be well understood so that a potential threatening tank with active armour be defeated effectively.

Therefore, to better understand the flight dynamics of projectiles flying in formation, DREV initiated a free-flight experimental programme to study the aerodynamic interference effects of two finned projectiles flying in a tandem configuration. The projectiles consisted of a four-fin cone-cylinder with a length-to-diameter ratio (l/d) of 6. Part of the aim of the study was to develop the necessary sabot technology so that a controlled separation could be achieved naturally. The other aspect was to obtain detailed trajectories of the projectiles to study interference effects. A series of free-flight tests were conducted at Mach 2 to verify a sabot design that was used to launch tandem projectiles, of similar configuration and size, from a 110 mm smooth bore. Four shots were fired, two at an open range to test the sabot functioning and model-sabot integrity at launch, and two in the DREV aeroballistic range. The sabot separation process, the measured trajectories, including the separation aspects of the trailing projectile relative to the leading one, are analysed and discussed. The stability of the models and their aerodynamic characteristic are compared relative to each other and with the results of a same configuration fired individually. Detailed flow photographs showing the complex shock wave structure and their interference on both models flying in close proximity are also given.

This initial study shows the extreme difficulty of firing two projectiles and having them fly in a controlled manner with no guidance. Even though preliminary, further tests should be carried out at higher Mach numbers where in service rounds are fired at. The use of guidance of the trailing projectile, and their required size to meet the future CF requirements should be pursued.

UNCLASSIFIED
vii

## NOMENCLATURE

| Variable | Computer Output | Description |
|---|---|---|
| d | | Diameter of projectile (mm) |
| $C_D$ | CD | Total drag coefficient |
| $C_{D0}$ | CD0 | Drag force coefficient at zero angle of attack |
| $C_{D_{\bar{\delta}2}}$ | CDSQ | Yaw drag coefficient derivative |
| c. g. | CG | Center of gravity |
| $C_{lp}$ | | Roll damping moment coefficient |
| $C_{ld}$ | | Roll moment coefficient due to fin cant |
| $C_{N\alpha}$ | CNa | Normal force coefficient slope |
| $C_{M\alpha}$ | Cma | Static pitch moment coefficient slope |
| $C_{Mq}$ | Cmq | Pitch damping moment coefficient |
| $C_{x0}$ | - | Axial force coefficient at zero angle of attack |
| | - | |
| $C_{x\alpha2}$ | - | Yaw axial force coefficient |
| $I_x, I_y$ | - | Axial and transverse moments of inertia |
| l | - | Length of projectile (m) |
| l/d | - | Length to diameter ratio |
| m | - | Mass of projectile (kg) |
| M | - | Mach number |
| $Re_l$ | - | Reynolds number based on length of projectile |
| | - | |
| $s_x$ | SX | downrange separation distance between projectiles (m) - (+ when trailing projectile is behind leading projectile) |
| $s_y$ | SY | cross range separation distance between projectiles (m) - (+ when trailing projectile is to the right of leading projectile) |
| $s_z$ | SZ | vertical separation distance between projectiles (m) - (+ when trailing projectile is below leading projectile) |
| | - | |
| V | - | Total projectile velocity (m/s) |
| $V_{muz}$ | - | Muzzle velocity (m/s) |
| X, Y, Z | - | Projectile coordinates (m) |
| t | - | Time of flight (s) |
| $\bar{\alpha}$ | - | Total angle of attack (deg) |

viii

| | | |
|---|---|---|
| $\overline{\alpha}_{max}$ | - | Maximum angle of attack (deg) |
| $\theta, \psi, \phi$ | THETA, PSI, PHI | Projectile orientation (deg) |
| $\overline{\delta}^2$ | - | Mean squared yaw (deg$^2$) |
| 6DOF | - | Six degree of freedom |

superscript

$\overline{s}$                                      s/d

UNCLASSIFIED
1

## 1.0 INTRODUCTION

There has been a great deal of interest recently in the flight dynamics and aerodynamic characteristics of projectiles flying formation in the low to high supersonic regime. The extent of application for these type of projectiles can range from tank APFSDS munitions to counteract active armour to multiple rocket flechette warheads where up to 100 flechettes are released simultaneously, or as in the case for FAT warhead with the RLU-5002/B rocket system where five flechettes are released at rocket burnout. In the first and last applications, the flechettes fly towards a target in a "cloud" formation. In this type of application, there is mutual aerodynamic interference acting on the projectiles depending on their location inside this cloud. The dispersion and the flight path will certainly be affected by the aerodynamic interference of one projectile on another depending of their proximity, and create higher angles of attack than desired. On the other hand, to counteract a vehicle with an active armour defense system, an optimum separation distance will be required between the leading and trailing projectiles to activate the defense mechanism and defeat the main armour. The tandem projectiles will have to be fired in one shot with minimal disturbances to have a low dispersion at the target, to separate from each other (naturally or otherwise), and to fly toward the target in formation. Ideally, the trailing projectile would fly in the wake of the leading one.

Some recent studies in the open literature (Refs. 1-8) make reference to various forms of projectiles flying in formation. One of these studies, Ref. 1, describes a computational study and the effect of reactive and active armour on projectiles in a tandem configuration. The advantages and disadvantages of naturally and forced separations are looked at from the point of view of optimal range engagement. A computational analysis to determine the aerodynamics of small cylinder segments flying in the wake of a bigger flared projectile at a Mach number of 4.4 was considered in Ref. 2. The drag coefficient is presented as a function of the separation distance between the parent projectile and the cylinder in the wake. Ballistic range tests were conducted (Ref. 3) on the separation of a subcalibre projectile at the base a flared parent projectile for speeds ranging from supersonic to hypersonic. They reported on the various mechanism that were used to separate the bodies and measured the

2

separation velocities. Various shadowgraph pictures are shown of the projectiles separating as they traveled downrange. A fourth study (Ref. 4) reports on results of wind tunnel experiments and a computational investigation of two projectiles in a tandem configuration at Mach 2. The trailing projectile in this case was of the same, and half the caliber of the forward projectile. The nose length of the aft projectile was varied. Flow visualization of the flow-field between the aft- and forbodies as well as static pressure measurements from wind tunnel tests were carried out. These results are compared with 3D Navier Stokes code predictions. The computed drag is given as a function of the separation distance. More complete results and analysis for this case can be found in Refs. 5 and 6. Ref. 7 conducted a computational fluid dynamics investigation of a tandem projectile configuration at approximately Mach 5. The leading and trailing projectiles were of the same calibre. The trailing projectile had a hemispherical nose shape while the leading projectile had conical and hemispherical nose shapes. The computations were conducted at zero angle of attack for various separation distances and the drag coefficients were computed and compared. The trailing projectile was also put off-axis in a vertical plane and the moments and forces on the trailing projectile were calculated for various off-axis distances, again at zero angle of attack.

Most of the studies mentioned above do not include free-flight tests to examine in detail the trajectories or the free-flight aerodynamic interference effects that two projectiles flying in close proximity could encounter. They are limited mostly to computational and wind tunnel investigations. All of the configurations that were investigated above also have no fins as a stabilizing feature. Some classified studies (Ref. 8) have been carried out on the flight dynamics of a tandem projectile configuration, but the results are not readily available.

Therefore, to better understand the flight dynamics of projectiles flying in formation, DREV initiated a free-flight experimental programme to study the aerodynamic interference effects of two finned projectiles flying in a tandem configuration. The aim of the study was to develop the necessary sabot technology so that a controlled separation could be achieved naturally. The challenge was to also modify, if possible, an existing sabot that was used to fire one projectile alone, to save cost. After the tandem sabot design

UNCLASSIFIED

3

successfully tested, full scale aeroballistic range tests were carried out to attempt in quantifying the aerodynamic interference effects of these finned projectiles flying in a tandem configuration. These are compared with results from aeroballistic range tests that were conducted at DREV on the same projectile configuration (Ref. 9) when fired individually. The free-flight results from this report constitutes a data base that could be used to validate wind tunnel tests and computational fluid dynamics studies.

The finned projectile configuration that was used for the tandem configuration was chosen since it was extensively tested in wind tunnels (Ref. 10), in free-flight in the DREV aeroballistic range (Ref. 9) and computationally (Ref. 11). The Mach number ranged from 2 to 4 for the computational and wind tunnel studies and from Mach 2 to 6.5 for the free-flight tests. A comparison of the results at Mach 2 from these three references can be found in Ref. 12. This choice of configuration would allow to characterize any interference effects in the tandem configuration on a well established and comprehensive existing data base.

The purpose of this memorandum is treefold: firstly, the sabot design and principle that was used to launch tandem projectiles of similar configuration and size are explained; then, the tests that were conducted to verify the sabot functioning and sabot-model integrity when launched at approximately Mach 2 at an open range are described and lastly, the aerodynamic characteristic of the tandem projectile configuration obtained from the DREV aeroballistic range are presented. A total of four shots were fired, two at an open range over a range of 100 m to verify the sabot launch and two in the DREV aeroballistic range over a range of 260 m. The sabot separation process is analysed and discussed. The optimum charge, chamber pressure, muzzle velocity and the projectile acceleration in the launch tube were acquired at the open range tests. The stability of the models was verified and the position of the second projectile relative to the first one was measured at both test sites as the projectiles flew downrange. The complete trajectories of both projectiles fired in the aeroballistic range and their aerodynamic characteristics are investigated. The aerodynamic results are then compared with the ones obtained when this projectile configuration was fired individually.

4

Detailed flow photographs showing the complex shock wave structure and their interference on both models flying in close proximity are also given.

This work was performed at DREV in 1993 under PSC 31D, Weapon Systems.

## 2.0 EXPERIMENTAL SITES AND INSTRUMENTATION

### 2.1 Open range site

The open range trials were conducted at one of DREV's open ranges parallel to the aeroballistic range. One of the four available butts (Butt-3) was utilized. A schematic of the test set-up is shown in Fig. 1 and a photograph of the test site is shown in Fig. 2. A sabot trap was installed at approximately 10.0 m from the gun muzzle so as to duplicate the launch configuration at the aeroballistic range. Two high speed photographic stations were positioned at 6m and 12 m, (for and aft of the sabot trap) and one at 50 m from the gun muzzle to photograph the sabot separation and model integrity. A cardboard target was situated at 100 m from the muzzle. Yaw cards were also placed along the flight path at 25 m, 50 m and 75 m from the gun muzzle. These were used to verify the model integrity, stability of the models and to measure the deviation of the second projectile relative to the first one. All the projectiles were fired from a 110 mm smooth bore gun.

Two radars were utilized for these tests. One to obtain the acceleration of the sabot-model package inside the gun tube and a second to obtain the velocity history of the projectile. The detail configuration and location of the radars are shown in Fig. 1. The acceleration in the gun tube was measured by a continuous Doppler type radar with a transmission frequency of 30 GHz. It was placed behind the gun and aimed at a metalised mylar radar signal reflecting mirror placed in front of the sabot trap. The mirror was situated to the side of the firing line to avoid model disturbance or damage and oriented towards and inside the gun muzzle. The data analysis was then conducted with an FFT analysis to obtain the velocity and acceleration histories.

5

The projectile velocities were measured with a continuous Doppler type radar (ED-850) with a frequency of 10.49 GHz. This radar was situated passed the sabot trap looking downrange and 1.0 m below the line of fire. It was aimed one meter above the target so as to capture the model radar signal as quickly as possible. The projectile velocity histories, their muzzle velocities and drag coefficients were obtained from this radar. The signal processing was also conducted with an FFT analysis.

The chamber pressures were measured with crusher gauges placed in the cartridge case.

## 2.2 Aeroballistic range

The DREV aeroballistic range (Refs. 13 and 14) is an insulated steel-clad concrete structure used to examine the exterior ballistics of various free-flight configurations. The range complex consists of a gun bay, a control room and the instrumented range. A massive blast wall is located in front of the building to stop sabot pieces and minimize vibrations transmitted to the range structure and instrumentation. Projectile of calibres ranging from 5.56 to 155 mm, including tracer types, may be launched. Large-caliber models have been fired up to Mach 7.

The 230-meter instrumented length of the aeroballistic range has a 6.1-m square cross section with a possibility of 54 instrumented sites along the range (Fig. 3). For these tests all stations were operational. These sites house fully instrumented orthogonal shadowgraph stations that yield photographs of the shadow of the projectile as it flies down the range. The maximum shadowgraph window, an imaginary circle within which a projectile will cast a shadow on both reflective screens, is 1.6 meters in diameter. There are also four Schlieren stations (three operational for these tests) at the beginning of the range that yield high-quality flow photographs. The range is also air-conditioned to maintain a constant relative humidity of approximately 45%. The nominal operational conditions of the range are 20°C at standard atmospheric conditions. The spark source and reference point locations that

6

were used were deduced from a standard survey. A dynamic calibration was conducted only in the downrange coordinate.

## 3.0 MODELS, SABOTS AND TESTS CONDITIONS

### 3.1 Model Configuration

The two projectiles that were used in tandem were exactly of the same configuration and based on Refs. 9, 10, 11 and 15. They consisted of a 28.07° nose cone on a cylindrical body with four clipped delta fins as shown in Fig. 4. There is a small recess (0.98 cal) in the diameter in front of the fins for a length of 1.75 calibres. There is also a large cavity at the base of the projectile (0.65 cal x 2.83 cal) as shown in the figure. The l/d of the model was 6. The fins had no leading edges and had a thickness of 0.085 calibres. The models were designed to obtain a center of gravity at approximately 3.4 calibres aft of the projectile nose. There was no deliberate canting of the fins to produce roll motion. The nominal diameter of the models was 20 mm. The models were modified by the addition of roll pins to aid in measuring the projectile's roll orientation in the aeroballistic range.

The physical properties of the models tested at the open range are given in Table I. Only one model was completely measured. The masses of the projectiles and their respective position inside the sabot are given in Table II. The physical properties of each projectile tested in the aeroballistic range are given in Table III. Care was taken in making sure that the lightest projectile was located at the back of the sabot, as the lighter model would decelerate faster, if there were no interference effects. Trajectory simulations, assuming no interference effects, indicated that a mass difference of only 4 g in the models would have a separation of 15 calibres at 240 m (the aeroballistic range distance), when both fired with an initial velocity of 688 m/s (Mach 2).

The numbering scheme to refer to the shots and a particular projectile is as follows. The individual shots will be labeled TD with a number to identify the shot. For example, TD-1 refers to the first shot. If not referred to specifically,

the front model will be labeled by a "J" and the second projectile by a "K" followed by a specific shot number. The projectiles are numbered by their initial positions in the sabot. For example DJ03 refers to the front model of the third shot fired. The "D" implies that a dynamic calibration was utilized for this shot. Other numbers indicating the date, (year, month, and date fired) are also used. For example, DK93051303, refers to an aeroballistic range test, fired on 13 May 1993, and is the back model of the third shot.

The models used in these initial tests were not high quality made models that are usually used in aeroballistic range tests. They were rebuffed models that had minor manufacturing faults. The major differences in the configuration from the previous tests (Refs. 9, 10, 12 and 15) were the small diameter recess and the fins leading edges. The leading edges of the models tested for this report were blunt while the previously tested models had a 30° conical leading edge. Since the primary goal of these trials was to verify the sabot launch and to attempt to obtain separation distances by differential aerodynamic forces, these minor inconveniences were deemed acceptable. Care should however be taken when comparing the aerodynamic results from these tests with previous ones.

The projectile configuration used for the tandem study was successfully fired individually in a Mach number range of 2 to 6.5 in the DREV aeroballistic range and the results can be found in Ref. 9.

## 3.2 Sabot design for tandem projectile

The tandem projectile sabot (Fig. 5) was designed to launch two projectiles of the same configuration, size and approximate physical properties from a 110 mm smooth bore gun. The sabot design for the tandem projectile configuration consisted of a two stage sabot with a Teflon coating. The working principle was simply to mechanically superimpose and unite two sabots of an existing configuration (Ref. 16) as shown in Fig. 6, which, when traveling in the gun tube, acted as a single stage sabot. At the gun muzzle, the forward stage broke the juncture from the rear sabot followed by the rear stage sabot

separation. This was to be accomplished without axial or lateral disturbance of either models.

A schematic of a plan view and 3-D cut-out view of the tandem sabot are shown in Fig. 7 and 8 respectively. As shown in those figures, the forward portion of the rear sabot (stage-2) engages a close fitting process at the base of the front portion (stage 1) of the sabot. The cantilever geometry of the forward portion of the 2nd stage supports and transmits the total mass of the front sabot and front projectile to the rear sabot wall and base. Four soft aluminum shear pins lock the sabot stages together. The rear tandem model base sits in a centering recess of the rear sabot while its conical nose protrudes the 1st stage rear portion. It is self-centered in a conical hole that matches the nose cone angle. The pointed nose of the rear model also protrudes inside the front tandem model base cavity without making contact with it. The nose of the trailing projectile protrudes 17.76 mm or 0.888 calibres inside the cavity of the front model. The forward model base is also centered in a recess while four cantilever supported centering screws line up the front of the model.

The 2nd stage inner cavity connects with that of the 1st stage through six holes to allow an equal air pressure build-up in both sabot cavities to activate the separation process.

The tandem sabot was of a two petal type and saw cuts were applied to both stages of the sabot. A sabot base pad seal was also used to prevent gas leakage pass the sabot body. The total launch mass of the tandem sabot-projectile was approximately 2.7 kg. The detailed drawings of the tandem sabot design are given in Annex A.

The details of the sabot integrity trial to launch only one projectile can be found in Ref. 16.

3.3 <u>Firing conditions</u>

A total of four tandem configurations were fired during these test trials. The initial Mach number of interest was 2 and all the firings were conducted at an approximate muzzle velocity of 700 m/s. Two shots (TD-1 and TD-2) were conducted at a proof range (Butt - 3) and two (TD-3 and TD-4) at the aeroballistic range complex. The atmospheric conditions at the open test site and at the aeroballistic range at time of firing are given in Table IV.

The models were mounted in the sabot so that the fin position of the first model was at 45° with respect to the rear model except for the TD-4 shot fired in the aeroballistic range. This shot had the fins aligned. One of the fins of the models located in front was painted blue for the outside trials. This was done so as to be able to measure the relative position of the second model with respect to the first on the yaw cards. Roll pins were utilized on the models for the aeroballistic range trials to measure the roll orientation of the models.

All the tests were conducted with N-3-1-1 (0.0353") propellant with the DREV 110 mm smooth bore gun. This propellant was well suited to obtain the muzzle velocities that were desired. The results of the gun launches are given in Table V. The chamber pressures given is the average of two British crusher gauges Mark IV with "E" conical coppers placed in the cartridge case. The accelerations were measured with a radar looking down the barrel through a reflector and only the maximums achieved are reported. The muzzle velocity and Mach number achieved for a charge mass of 0.794 kg are also given. The maximum accelerations measured were approximately 8 000 gn.

## 4.0 <u>SABOT SEPARATION and FUNCTIONING</u>

All the sabots functioned very well. Fig. 9 and 10 show high speed camera photographs at two positions (before and after the sabot trap) for the two shots that were fired at the open range test site (Fig. 1). As can be seen, the sabot separation is quite acceptable and the sabot petals clear the projectiles without disturbing them. The projectiles are also separating naturally and without contact. Photographs from a third camera that was

located at 50 m from the muzzle to photograph mainly the separation in the downrange coordinate were not successful due to a synchronization problem.

High speed photographs, taken at 4.5 m from the muzzle of the gun, of the sabot separation process for shots TD-3 and TD-4 fired in the aeroballistic range are shown in Fig. 11 and 12, respectively. Again good separation was obtained for these two shots at a Mach number of 2. The trailing projectile of the TD-4 shot (Fig. 12) appears to be in the base cavity of the leading projectile. The aligned fins of both models are clearly seen on the photograph.

Schlieren photographs obtained in the aeroballistic range at approximately 20 m from for the muzzle are given in Fig. 13. Complex shock structures and mutual interference are easily discernible.

These photographs attest that the sabot design is quite adequate to launch two projectiles of the same configuration and size at a test velocity of approximately 710 m/s. There were no breakage of the sabot and no contact between the sabots pieces and the models. The sabot separation process was quite repeatable. Initial stress analyses have shown that this tandem sabot design configuration, with the present projectiles, could be fired up to approximately Mach 4.

## 5.0 MODEL SEPARATION TRAJECTORY ANALYSIS

The measured experimental trajectories of the tandem models will be analyzed and discussed. The measured trajectories for the open range trials were very limited since only four yaw cards were used. The aeroballistic range data was more complete, provided longer trajectories and they were more accurate. Most of the results discussed will be the separation distances and the pitch-yaw attitude of the aft model relative to the first one for the four shots.

The terminology and sign convention used is explained in Fig. 14. The separation in X between the two models, $s_X$, is the distance between the nose tip of the trailing projectile behind the base of the leading projectile. A negative $s_X$ implies that the trailing projectile is overtaking the leading one. The

separation distances in the Y and Z directions, $s_y$ and $s_z$, respectively, are the distances between the position of the center of gravity of the trailing projectile relative to the leading one.

## 5.1 Outside trials

The position of the second projectile relative to the first one was measured at the four yaw cards located downrange of the gun as shown in Fig. 1 and these are given in Table VI. Only the results in the cross range coordinates (Y and Z) were possible at this test site. The TD-1 models basically remained in line, less that one calibre separation, up to 100 m. The rear projectile of shot TD-2 remains 1 calibre to the right of the first one and slips below the flight path of the first one as they travel downrange, to a maximum of three calibres at 100 m.

All the yaw cards were also inspected and it was concluded that all the models were intact and stable.

The velocity history of the projectiles were also measured with the radar looking downrange (Fig. 1). During the FFT analysis it was possible to differentiate the two projectiles in flight from the radar as shown in Fig. 15. The two pulses that are seen represent the frequency shift from the two projectiles. The drag coefficients were also deduced from the velocity histories and these will given in the next section.

## 5.2 Aeroballistic range trials

The main objective of conducting tests in an aeroballistic range is to determine a projectile's free-flight aerodynamic characteristics. These aeroballistic coefficients and stability derivatives are determined by analyzing the measured trajectories of a projectile in flight at a number of photographic stations in the range. The precise measurements that are required are the projectile's center-of-gravity position, its orientation, plus the time of spark

12

discharge at every station (t, X, Y, Z, $\theta$, $\psi$, $\phi$). These are obtained by reading various critical points (nose and tail) of the projectile's shadow on films and they are numerically coded on a microdensitometer relative to a reference system. The trajectory is then calculated by assuming that the exact position of the spark sources and the reference markers at each station in the aeroballistic range coordinate system are well known. The total flight distance in the aeroballistic range is approximately 260 m. The roll pins were not readable or discernible due to the interference of the shadow of one projectile over the other. Therefore, no roll data was obtainable.

### 5.2.1 TD - 3 SHOT

The experimental trajectories for shot TD-3 are given in tabular form and graphical form as a function of the downrange distance in Annex B. The trajectories of both the front and back models are on the same graphic to better visualize the separation process of one projectile relative to the other. The experimental data points are given as circular and the solid lines are there only to connect the experimental data points to better visualize the overall trends.

There was only data (Annex B) for the first 23 stations (85 m) for the front model (DJ03) and up to 190 m for the trailing projectile (DK03). The TD-3 second projectile separated quite quickly from the first one and in all directions. Even at the Schlieren stations (22 m), it was way off line in the Y-direction. At approximately the 8th window (50 m), the second projectile surpassed the first one. At this stage the first projectile was at the extreme left of the firing window.

The position of the second projectile relative to the first one is given in Fig. 16 in calibres for the first part of the trajectory where both projectiles can be seen on the same photographs. Fig. 17 shows a series of shadowgraph pictures (pit and wall views) of both projectiles on the same film, at various positions downrange. The second projectile starts to overtake the front model (negative $\bar{s}_x$, Fig. 16 a) at the first station. At approximately 50 m downrange, both projectiles are at the same downrange position ($\bar{s}_x$ = -6 calibres) and at 75

UNCLASSIFIED

13

m it has completely overtaken it by one projectile length. The separation distance in the X direction (downrange) between the two projectiles continues to increase as both projectiles travel downrange. At the first stations, the first projectile did have a bit of yaw while the second did not seem to have any (Fig. 17). This would impart a higher retardation force to the first projectile which would decelerate faster that the second one.

Shock wave interference of the leading projectile on the trailing projectile can be clearly seen in Fig. 17 on the P2 view. The bow shock of the leading projectile impacts the fins of the trailing projectile. There seems to be no other shock wave interference from the 8th window on. A shock wave can also be clearly seen emanating behind the nose of the projectile where the diameter of the projectile recesses.

The separation in the Y- and Z - directions are shown in Fig. 16 b and c, respectively. At 90 m, the second projectile is approximately 22 calibres to the right of the front model, when viewed from the rear (Fig. 16 b). The projectile was no longer seen on the shadowgraphs as it was outside the firing window. The second projectiles' flight path is approximately 2.5 calibres below the first one at 90 m (Fig. 16 c) in the Z direction.

The pitch and yaw motions of both projectiles are given in Annex B. The yaw motion (PSI) is very high for the front projectile, DJ03, and varies between -15° to 10° while the second projectile's yaw motion ranged between -4° to +4°. The overall pitch motion ($\theta$) is lower in magnitude, with the back model having a higher magnitude. Both motions damp out as seen in the figures. The wavelength of the motion is approximately 20 m. These wavelengths of the angular motion are the same as the projectiles that were individually fired at the same Mach number (Ref. 9).

14

### 5.2.2 TD - 4 SHOT

The measured trajectories, with the time of flight, for this shot, are given Annex C in the same format as the previous shot. Experimental data was obtainable only up to 110 m before both projectiles were outside the firing window.

The TD-4 shot showed a completely different behavior from the first three shots. The nose of the second projectile remained in the base cavity of the first one for the whole length of the range. It should be noted that the fins for this case were initially aligned in the sabot while for the other shots they were 45° offset. Some minor displacements and angular motion of the second projectile with respect to the first one were visible, but the nose of the second projectile always remained in the cavity at the base of the first projectile for the length of the range (Fig. 13 b). This can also be seen at 4.5 m from the muzzle (Fig. 12).

The position in the downrange coordinate of the second projectile relative to the first one is given in Fig. 18 in calibres. The nose of the rear model protruded inside the first one by approximately 1.2 calibres. An expanded view is given in Fig. 18 b in terms of mm. If there is physical contact between the two models, from the geometry of the nose and the base cavity (Fig. 4) of the projectiles, the maximum distance that the nose of the trailing projectile can protrude in the base cavity of the front one is 26 mm or 1.3 cal. It appears that up to 50 m, there was no contact but beyond that, there was physical contact. The variability in the data is due to reading difficulties and positional inaccuracies in the reference system and spark source locations. The overall trend is still adequate and indicative.

It should be noted that when fired, the projectiles were not in physical contact. The sabot design (Fig. 7) prevents any contact between the two models. The back model protrudes 17.78 mm in the cavity of the front model in the sabot. The back model had a lighter mass than the front one by 0.7 g. Without interference effects, it should have decelerated faster than the front one. The second projectile was probably sucked in the first one due to the lower

base pressure in the cavity and the recirculation region at the base of the leading projectile (Ref. 4).

The relative positions in the cross range coordinates (Y and Z) of the second projectile relative to the first one are given in Fig. 19. The center of gravity of the aft projectile is initially to the right (Fig. 19 a and Annex C) by 0.3 cal relative to the front one at 30 m, swings to the left to 0.3 cal and returns to the right again to 0.3 cal. A typical behavior in the Z direction is also seen (Fig. 19 b and Annex C). The center of gravity of the aft projectile is lower relative to the first one initially by 0.75 cal, and moves higher relative to the first one by 0.5 cal at approximately 60 m and moves again lower by 0.25 cal further downrange.

The angular motions in the pitch (THETA) and yaw (PSI) planes are given on the same graph for both the front and back models in Annex C and are compared relative to each other in Fig. 20. The front projectile (DJ04) pitch motion varies from +8° to -5°. The back model's pitch motion ($\theta$) is initially a bit higher but at approximately 50 m it is of the same amplitude and phase as the front model (Fig. 20a). The yaw motion ($\psi$) of the front model is lower than the pitch motion but is of the same frequency (Annex C). The back model swings to the left and right relative to the first one by ±1° with a wavelength of approximately 40 metres (Fig. 20b).

## 5.3 Comparison of shots

The flight path of the projectiles fired to proof test the tandem sabot (shots TD-1 and TD-2) at the open range seem to remain more in line with respect to one another, when compared with the shots fired in the aeroballistic range (shots TD-3 and TD-4).

The setups for the initial part of the trajectory were a bit different for the two trials. At the aeroballistic range complex, there are baffles between the sabot trap wall and the opening of the range to redirect any blast from the gun. There were no such obstructions pass the sabot trap at the open range. The TD-3 shot projectiles fired in the aeroballistic range separated very quickly

from each other as compared to the TD-1 and TD-2 shots fired at the open range. The setups in the sabot were identical for the three shots. The trial setup could account for some of the differences in the separation process. For example, shock waves from the leading projectile could have reflected off the baffles or the entrance hole in the range, and impact the trailing projectile asymmetrically enough to change its attitude and consequently, its flight path.

The only shot (TD-4) where there was no clear separation between the two models was the only shot where the fins of the two models were initially aligned in the sabot. The other three shots had the fins at 45° apart. The airflow over of the fins of the rear model in the 45° setup was definitely higher than the in line configuration. This difference in incremental drag was probably enough to have the models separate cleanly while the in-line fin models did not have enough incremental drag differences to achieve natural separation.

## 6.0 AERODYNAMIC CHARACTERISTIC

The aerodynamic data obtained from the open range tests was limited to the drag values since only the velocity histories were obtained from the radar. A more complete aerodynamic analysis was possible from the aeroballistic range trials as a complete trajectory was obtained to reduce to aerodynamic coefficients. No roll data was available since the roll pins were not readable.

### 6.1 Free-flight data reduction

Extraction of the aerodynamic coefficients and stability derivatives is the primary goal in analyzing the trajectories measured in the DREV aeroballistic range. This is done by means of the Ballistic Range Data Analysis System (BARDAS, Ref. 17) shown in Fig. 21. This program, BARDAS, incorporates a standard linear theory and a six-degree-of-freedom (6DOF) numerical integration technique. The 6DOF routine incorporates the Maximum Likelihood Method (MLM) to match the theoretical trajectory to the experimentally measured trajectory. The MLM is an iterative procedure that adjusts the aerodynamic coefficients to maximize a likelihood function. The

application of this likelihood function eliminates the inherent assumption, in least-square theory, that the magnitude of the measurement noise must be consistent between parameters (irrespective of units). In general, the aerodynamic coefficients are nonlinear functions of angle of attack, Mach number and roll angle.

BARDAS represents a complete ballistic range data reduction system capable of analyzing both symmetric and asymmetric models. The essential steps of the data reduction system are (1) to assemble the dynamic data (time, position, angles), model measured physical properties and atmospheric conditions, (2) to perform linear theory analysis, and (3) to perform 6DOF analysis.

These three steps have been integrated into BARDAS to provide the test scientist with a convenient and efficient means of interaction. At each step in the analysis, permanent records for each shot are maintained so that subsequent analyses with data modification are much faster.

The 6DOF data reduction system can also simultaneously fit multiple data sets (up to five) to a common set of aerodynamics. Using this multiple-fit approach, a more complete range of angle of attack and roll orientation combinations is available for analysis than would be available from a single flight. This increases the accuracy of the determined aerodynamics over the entire range of angle of attack and roll orientations.

The aerodynamic data presented in this document were obtained using the linear theory analysis, the fixed-plane 6DOF analysis (MLMFXPL) with the single fit data correlation techniques after a dynamic calibration, as discussed below. The equations of motion have been derived in a fixed-plane coordinate system assuming a rigid body, with Coriolis effects included. The formal derivation of the fixed-plane model is given in Ref. 18.

All the results shown here were reduced after the dynamic calibration biases were accounted for in the X-direction. The details of the dynamic calibration for the DREV aeroballistic range are given in Ref. 9 and the methodology is explained in Ref. 19.

18

## 6.2 Open range drag coefficient

Only the drag coefficient was obtainable from these trials. A FFT analysis was conducted on one of the traces of the radar (Fig. 15). Since the trajectory of the models were more or less in line (Table VI) and the radar was looking downrange, it can be assumed that the determined drag coefficients were for the trailing projectiles. The determined total drag coefficients for this trial are given in Table VII.

There were slight differences in the determined drag coefficients. These might be due to angle of attack variations effect on $C_D$ and not exactly knowing which of the projectiles (leading and trailing) the FFT traces belong to.

## 6.3 Aeroballistic range

### 6.3.1 TD-03 SHOT

The complete measured trajectories for the projectiles of Shot TD-3 could not be used for a reliable aerodynamic analysis. The shadows of the projectiles overlapped for the first 19 windows when the back projectile surpassed the front one for this shot. Some guessing by the film reader was required to obtain the necessary points on the shadow of the projectiles. This was deemed acceptable to look at the general trends of the trajectories but was not considered acceptable for the determination of aerodynamic coefficients, due to possible high errors in reading. It was therefore decided to only use data past the 19th window to conduct the aerodynamic analysis. Since the DJ03 projectile went out of the firing window, where the projectile can be photographed on both views, a few stations further downrange, only the DK03 model could be analysed.

The linear results for this shot are given in Table VIII. The conditions at time of firing with the probable errors of fits from the linear theory analysis are given in Table VIIIa, the determined parameters in Table VIIIb and finally, the

19

reduced aerodynamic coefficients in Table VIIIc. The probable error of fits in the positional coordinates are quite acceptable (0.6 mm) but the errors in angles in the pitch and yaw plane are a bit high (0.5°).

The 6DOF reduced aerodynamic coefficients are given in Table IX. The probable errors of fits are equivalent to the linear theory ones. The maximum angle of attack observed was 4.7°. The 6DOF reduced normal force coefficient slope ($C_{N\alpha}$), the pitching moment coefficient slope ($C_{M\alpha}$) and the axial force coefficient slope ($C_{X0}$) were very well determined as evident by the very low probable errors in parentheses below the determined values. $C_{Mq}$ was not as well determined but is considered reliable. The linear theory and 6DOF - single fit reduced aerodynamic coefficients also agree quite well. These aerodynamic coefficients as well as those of the open range trial and Ref. 9 will be compared in section 6.4.

Annex D gives the observed motion and the theoretical determined one with these reduced aerodynamic coefficients. The experimental data points (open circles) and the calculated trajectory (continuous line) from the determined coefficients are compared. This allows a verification that the reduced aerodynamic coefficients do fit the experimental trajectory satisfactorily. For every shot, the total angle of attack, the velocity history, the swerve motion as well as the angular motion plots are given as a function of the downrange coordinate.

## 6.3.2 TD-04 SHOT

From the trajectory analysis of this shot, Section 5.2.2, it is quite evident that the rear projectile is in contact with the leading projectile for most of the measured trajectory. Specifically, the nose of the trailing projectile is in the base cavity of the front projectile and at a maximum. Also, the rear model has a motion slightly different from the front one. It acts as it was tethered projectile or a flexible one. The in-flight arrangement of these two projectiles resembles more of a missile configuration. When in contact, the configuration has two sets of fins, one set at the rear and the other at the mid-length of the "joined" projectile.

The yaw motion of the front projectile also dictates that this "combined" projectile has a quite different behavior than a projectile flying alone. The yaw wavelength of the DJ04 projectile is approximately 90 m. This is 3 times the yaw frequency of the projectile flying alone, as seen in Section 6.3.1 and Ref. 9.

This type of motion cannot be analysed with the present model in BARDAS which assumed rigid body dynamics. Some attempts at analyzing models that bend in flight with an elasticity model from free-flight tests were conducted in the past, Refs. 20, 21 and 22. These tools were not available at DREV and were outside the scope of these studies.

The determined drag coefficient of this "joined projectile", reduced with the linear theory analysis, was 0.88 for a mid-range Mach number of 1.95. The mass of the two projectiles were combined to achieve this drag value.

## 6.4 Comparison of aerodynamic results

Since there were no controlled separation in the aeroballistic range, where the trailing projectile remained in the wake of the leading projectile by a couple of calibres, it was not possible, unfortunately, to deduce any interference effects. Nevertheless, the aerodynamic coefficients determined from these trials are compared with those obtained from Ref. 9 in Table X. The reference center of gravity position for these comparison was taken to be at 3 calibres from the nose of the projectile, the same as Ref. 9. The test Mach numbers are slightly different, but this should not have a great influence on the aerodynamic coefficients.

The model tested (DK03) in this report has a higher axial force coefficient, by approximately 28%, when compared to the one tested in Ref. 9. This is mostly attributed to the thick fins of the models tested in these trials where they had no leading edges as compared to the ones tested in Ref. 9. The projectile tested here also has more static stability, ($C_{M\alpha}$), and the fins used here are more effective (higher $C_{N\alpha}$). The pitch damping coefficient, $C_{Mq}$, also agree quite well.

One of the radar determined drag (TD-2, Table VII) coefficient was consistent with the DK03 model. The other shot (TD-1) has a lower drag than the DK03 projectile. The TD-1 shot showed not much cross range separation between the two models (Table VI) and if the projectile was in the wake behind the leading projectile by a couple of calibres, it could explain the lower drag. This was predicted by computational studies depending on the separation distances (Refs. 4 and 7). But since there was no data for the separation in the downrange coordinate for this shot, it is difficult to conclude this point with certainty.

## 7.0  CONCLUSIONS and RECOMMENDATIONS

A set of initial trials to test a sabot design concept to launch similar finned projectiles to obtain the trajectories and aerodynamic characteristic at Mach 2 were successfully completed. Four projectiles were fired, two at an outside proof range and two in the DREV Aeroballistic Range. The propellant charges to obtain the desired velocities were determined, as well as the maximum accelerations and muzzle velocities. The separation distances of the second projectile relative to the first were also determined as well as the attitude. High quality Schlieren photographs were also obtained showing complex shock structures and interference.

All the tandem sabots functioned very well for the four shots fired. The tandem projectiles separated naturally for three shots and one remained in the base cavity of the lead projectile. This was the only shot where the fins of both models were initially aligned with each other in the sabot.

The measured experimental trajectories from the open range tests as well as those from the aeroballistic range were analysed and compared. Possible explanations for the different flight profiles from quick separation to contact of  one projectile in the base cavity of the leading projectile were also brought forward.

22

The complete aerodynamic characteristic of only one model was obtainable from the aeroballistic range since one model flew outside the firing window quite early in the trajectory for one shot, and the two models of another shot remained in contact. The interference effects could not be deduced from these tests. The reduced aerodynamic coefficients are compared with another series of trials and differences in the stability and axial force coefficient were attributed mainly to the slight differences in the fins on the configurations that were used.

Initial stress analyses have shown that the tandem sabot configuration with the present projectiles could be fired up to approximately Mach 4. Therefore, a possible next step of the project would be to fabricate more tandem sabots with high quality made models to verify the launch integrity at Mach 4. The goal of the aeroballistic range trials would be to characterize the aerodynamic interference effects as a function of the separation distances of the two projectiles in flight. A critical aspect in this type of testing is to have the trailing projectile fly in the wake of the leading projectile by approximately 2 to 10 calibres.

Wind tunnel force tests should be conducted at DREV on this tandem projectile configuration at Mach 2. The indraft wind tunnel facility has an upstream sting support as well as the traditional downstream support. The use of both supports at the same time could be used with the same projectile configuration as the one tested here. The advantage of the wind tunnel, in this case, is that the separation distances between the models can be set precisely and exactly in the wake of the upstream arrangement. The angles of attack of the trailing projectile on the downstream support, where force measurements will be taken, could then be varied. In this manner, the static aerodynamic coefficients as a function of angle of attack, roll orientation and separation distances could be quantified quite easily. Wind tunnel tests can also be conducted on the trailing projectile off-axis from the leading one and varying the angles of attack and separation distances.

UNCLASSIFIED
23

## 8.0 ACKNOWLEDGMENTS

The trials team of Armaments Division are thanked for their participation and execution of these tests which were conducted, as always, in a very professional manner.

UNCLASSIFIED
24

## 9.0 REFERENCES

1. Lehr, H. F. and Merkel, Th., "Computational Study on the Application of Tandem Projectiles in Different Distances of Engagement", 13th International Symposium on Ballistics, Stockholm, Sweden, 1-3 June 1992

2. Sahu, J., and Nietubicz, C. J., "A Computational Analysis of Cylindrical Segments in the Wake of a Projectile", 4th International Computational Fluid Dynamics, University of California, Davis, Davis, California, 9-12 September, 1991

3. Butler, G., King, D., Abate, G. and Lt. Stephens, M., "Ballistic Range Tests of Store Separation at Supersonic to Hypersonic Speeds", AIAA 91-0199, 29th Aerospace Sciences Meeting, Reno Nevada, 7-10 January, 1991

4. Berner, C., "Aerodynamic Interference Between Tandem Projectiles: Measurements and Computations", 14th International Symposium on Ballistics, Québec, Canada, 26-29 September 1993

5. Berner, C., Demeautis, C. and Duffner, P., "Vol supersonique de deux projectiles séparés par une faible distance. I.1 Visualisation des écoulements et mesures de pression autour de projectiles de références", ISL report, R 107/92.

6. Demeautis, C., Duffner, P., and Berner, C., "Vol supersonique de deux projectiles séparés par une faible distance. I.2 Mesures du champ des vitesses autour de projectiles de références", ISL report, R /93.

7. Ober, C. C., Lamb, J. P. and Kiehne, T. M., "A Computational Study of the Aerodynamics of a Body Immersed in a Supersonic Wake", AIAA-94-3519-CP, 1994

8. Garner. J. M. and Jara, E. A., "Aeroballistic Test of Tandem Rod Projectiles", ARL-MR-82, June 1993, SECRET

UNCLASSIFIED
25

9. Dupuis, A. D. and Hathaway, W. H., "Aerodynamic Characteristic of a Finned Projectile at Supersonic and Hypersonic Speeds from Free-Flight Tests", DREV R-9404/94, October 1994, UNCLASSIFIED

10. Berner, C., and Dupuis, A. D., "Wind Tunnel Investigation and Data Analysis of the DREV/ISL Reference Projectiles", DREV Report, in preparation

11. Berner, C., "Numerical Investigation of the DREV/ISL Reference Projectiles", DREV Report, in preparation

12. Dupuis, A. D. and Berner, C., "Experimental and Numerical Investigation of a Finned Projectile at Mach 2", 14th International Symposium on Ballistics, Québec, Canada, 26-29 September 1993, also published as ISL PU 348/93

13. Drouin, G., Dupuis, A. and Côté, F., "Instrumentation Development and Data Analysis for the DREV Aeroballistic Range", DREV M-2800/87, March 1987, UNCLASSIFIED

14. Dupuis, A. and Drouin, G., "The DREV Aeroballistic Range and Data Analysis System", AIAA Paper No. 88-2017, AIAA 15th Aerodynamic Testing Conference, San Diego, California, 18-20 May, 1988.

15. Hutt, G. R. and East, R. A., "Dynamic Pitch Stability Measurements of Slender Cone-Cylinder Finned Bodies at High Mach Number", 9th International Symposium on Ballistics, RMC, Shrivenham, UK, April 1986.

16. Dupuis, A. D. and Normand, M., "Sabot Performance for the Joint DREV-RARDE Hypersonic Cooperative Project", DREV M-3109/92, June 1992.

17. "Ballistic Range Data Analysis System (BARDAS)", Arrow Tech Associates Inc., DREV Contract No. W7701-0-1227, March 1992.

18. Hathaway, W. H. and Whyte, R., "Aeroballistic Research Facility Free-Flight Data Analysis using the Maximum Likelihood Function", AFATL-TR-79-98, December 1979, UNCLASSIFIED

19. Whyte, R. and Hathaway, W., "Dynamic Calibration of Spark Aeroballistic Ranges", 44th Aeroballistic Range Association Meeting, 13-17 Sept., 1993, Munich

20. Courter, R. W., and Thomas, K. H., "Preliminary Study of the Effects of Model Elasticity on Range-Acquired Aerodynamic Coefficients", Proceedings of the 38th Meeting of the Aeroballistic Range Association, Tokyo, Japan, 6-8 October, 1987

21. Courter, R. W., and Thomas, K. H., "Aeroelastic Effects on Range-Acquired Aerodynamic Coefficients", Proceedings of the 39th Meeting of the Aeroballistic Range Association, Albuquerque, New Mexico, 10-13 October, 1988

22. Courter, R. W., and Thomas, K. H., "Aerodynamic Coefficients Determined by a Generalized Elastic Body Regression Algorithm from Free-Flight Ballistic Range Data", Proceedings of the 40th Meeting of the Aeroballistic Range Association, Paris, France, 25-28 September, 1989

## TABLE I
## Typical physical properties of free-flight models

| | | |
|---|---|---|
| d | (mm) | 20.00 |
| $I_x$ | (g-cm$^2$) | 114.677 |
| $I_y$ | (g-cm$^2$) | 1562.75 |
| l | (cm) | 12.0 |
| CG | (cm from nose) | 6.68 |

## Table II
## Projectile mass and position in sabot

| Shot Number | Model Position | Model Mass (gm) |
|---|---|---|
| TD - 1 | Front - J01 | 176.0 |
| | Back - K01 | 177.0 |
| TD - 2 | Front - J02 | 177.0 |
| | Back - K02 | 177.0 |
| TD - 3 | Front - DJ03 | 177.3 |
| | Back - DK03 | 175.9 |
| TD - 4 | Front - DJ04 | 177.2 |
| | Back - DK04 | 176.5 |

## Table III
### Aeroballistic range tested projectile physical properties

| Projectile number | d (mm) | Mass (g) | $I_x$ (g cm²) | $I_y, I_z$ (g cm²) | l (mm) | CG (mm) | CG cal. from nose |
|---|---|---|---|---|---|---|---|
| DJ93051303 | 19.969 | 177.3 | 115.17 | 1562.48 | 120.05 | 68.785 | 3.445 |
| DK93051303 | 19.990 | 175.9 | 114.77 | 1566.45 | 120.00 | 68.489 | 3.426 |
| DJ93051304 | 19.989 | 177.2 | 114.77 | 1565.01 | 119.99 | 68.472 | 3.426 |
| DK93051304 | 20.002 | 176.5 | 113.81 | 1559.58 | 120.40 | 68.658 | 3.433 |

## Table IV
### Firing conditions

| Shot Number | Date Fired | Location of Test | Atmospheric Temp (°C) | Atmospheric Pressure (KPa) |
|---|---|---|---|---|
| TD-1 | 93-04-14 | Butt-3 | 7.0 | 99.69 |
| TD-2 | 93-04-15 | Butt-3 | 10.0 | 100.90 |
| TD-3 | 93-05-13 | A/B Range | 21.9 | 97.99 |
| TD-4 | 93-05-13 | A/B Range | 21.3 | 98.07 |

TABLE V

Results from gun firing with propellant N-3-1-1 (0.0353")

| Shot Number | Total Launch. Mass (kg) | Charge Mass (kg) | Chamber Pressure (MPa) | Maximum Acceleration (gn) | Muzzle Velocity (m/s) | Mach Number at Muzzle |
|---|---|---|---|---|---|---|
| TD-1 | 2.67 | 0.794 | 29.7 | 8 258 | 730.0 | 2.18 |
| TD-2 | 2.65 | 0.794 | 26.2 | 7 806 | 704.0 | 2.09 |
| TD-3 | 2.65 | 0.794 | 24.8 | - | 678.4 | 1.97 |
| TD-4 | 2.66 | 0.794 | 27.9 | - | 691.6 | 2.01 |

Table VI

Position of second projectile relative to the first one (open range test)

| | SHOT NUMBER | | | |
|---|---|---|---|---|
| | TD - 1 | | TD - 2 | |
| x (m) | $\bar{s}_y$ (cal) | $\bar{s}_z$ (cal) | $\bar{s}_y$ (cal) | $\bar{s}_z$ (cal) |
| 25 | 0.00 | 0.00 | 1.00 | 0.25 |
| 50 | 0.00 | 0.00 | 1.00 | 0.90 |
| 75 | -0.30 | 0.20 | 0.90 | 1.75 |
| 100 | 0.35 | -0.70 | 1.00 | 2.95 |

## Table VII
### Drag coefficient determined from radar velocities

| Shot Number | Mach Number | CD |
|---|---|---|
| TD - 1 | 2.134 | 0.527 |
| TD - 2 | 2.028 | 0.666 |

## Table VIII
### Linear theory results for Shot DK03

#### a) Conditions at time of firing

| Shot Number | No. of Stations | Observed Distance (m) | Air Density (kg/m3) | Speed of Sound (m/sec) | Reynolds Number (length) | X (m) | Probable Error Swerve (m) | Angle (deg) | Roll (deg) |
|---|---|---|---|---|---|---|---|---|---|
| DK93051303 | 27 | 115.0 | 1.15314 | 344.34 | 0.476E+07 | 0.0007 | 0.0004 | 0.436 | 0.00 |

#### b) Linear theory parameters

| Shot Number Damping | Mach Number | DBSQ Rate (deg**2) | Nutation Vector Rate [K10] (deg) | Precession Vector Accel. [K20] (deg) | Nutation Damping Accel. [L1] (1/m) | Precession Damping [L2] (1/m) | Nutation Frequency [W10] (deg/m) | Precession Frequency [W20] (deg/m) | Nutation Change [WD1] (deg/m2) | Precession Change [WD2] (deg/m2) |
|---|---|---|---|---|---|---|---|---|---|---|
| DK93051303 | 1.828 | 4.9 | 1.52 | 3.58 | -0.01474 | -0.01219 | 20.263 | -22.454 | 0.00000 | 0.00000 |

#### c) Aerodynamic coefficients

| Shot Number | Mach Number | DBSQ | CD | CD0 | CDSQ | CNa | Cma | Cmq | Cmpa | Roll Fit Clp | Frequency Fit Clp |
|---|---|---|---|---|---|---|---|---|---|---|---|
| DK93051303 | 1.828 | 4.9 | 0.636 | 0.615 | 13.851 | 9.419 | -6.002 | -86.8 | 9.986 | 0.000 | 0.000 |

Table IX

Six degree of freedom aerodynamic coefficients - Shot DK93051303

| Mach Number | $\bar{\delta}^2$ $\bar{\alpha}_{max}$ | $C_{x0}$ $C_{x\alpha2}$ | $C_{N\alpha}$ | $C_{M\alpha}$ | $C_{Mq}$ | Probable Error | |
|---|---|---|---|---|---|---|---|
| | | | | | | X (mm) Y - Z (mm) | Angle (deg) Roll (deg) |
| | 4.1 | 0.620 (0.1%) | 9.08 (4.0%) | -6.524 (1%) | -90.8 (28%) | 0.7 | 0.49 |
| 1.83 | 4.7 | 4.432 (*) | | | | 0.5 | - |

Table X
Comparison of aerodynamic coefficients

|  | Ref. 9 | Shot DK03 |
|---|---|---|
| Mach Number | 1.99 | 1.83 |
| $C_{x0}$ | 0.483 (0.0%) | 0.620 (0.0%) |
| $C_{N\alpha}$ | 7.51 (4.0%) | 9.08 (4%) |
| $C_{M\alpha}$ | -6.414 (0.%) | -10.356 (1.%) |
| $C_{Mq}$ | -80.0 (-) | -90.8 (28%) |

UNCLASSIFIED
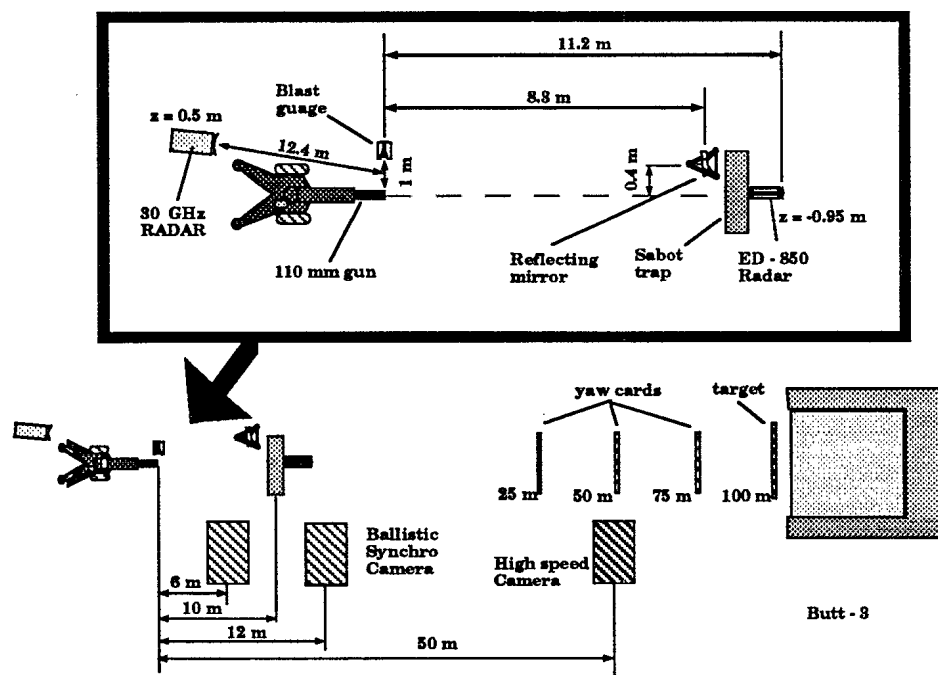


FIGURE 1 - Schematic of the open range test site



FIGURE 2 - Photograph of open range test site

UNCLASSIFIED



FIGURE 3 - Aeroballistic range photographic station spacing



FIGURE 4 - Model configuration (all dimensions in calibre)
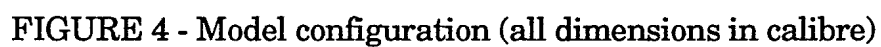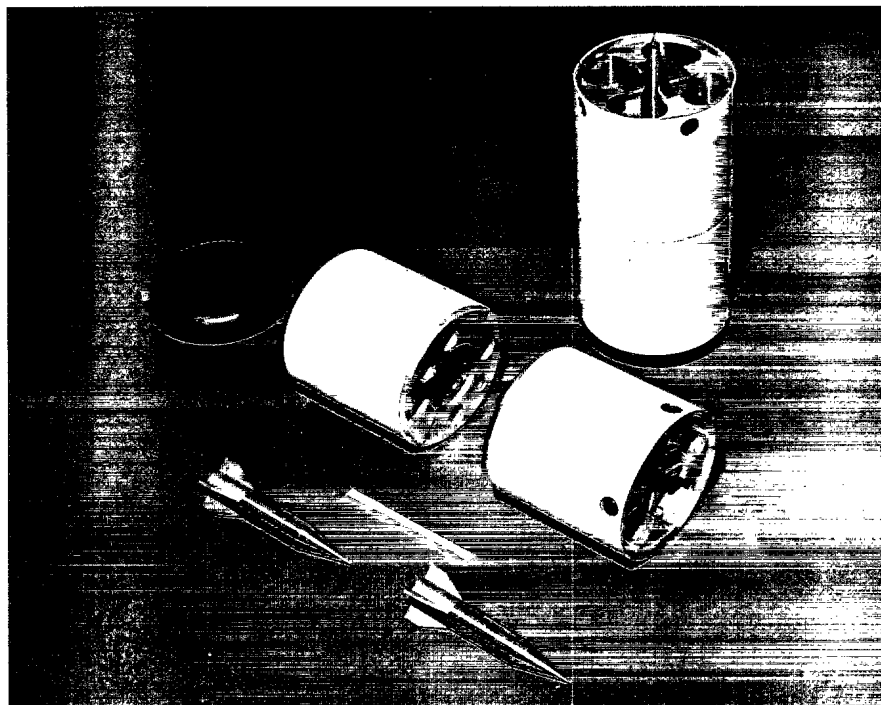
UNCLASSIFIED



FIGURE 5 - Photograph of tandem sabot and models



① SEAL
② SABOT
③ LINER TEFLON
④ SCREW (REWORKED)
⑤ MODEL
⑥ PAD
⑦ PAD SCREW
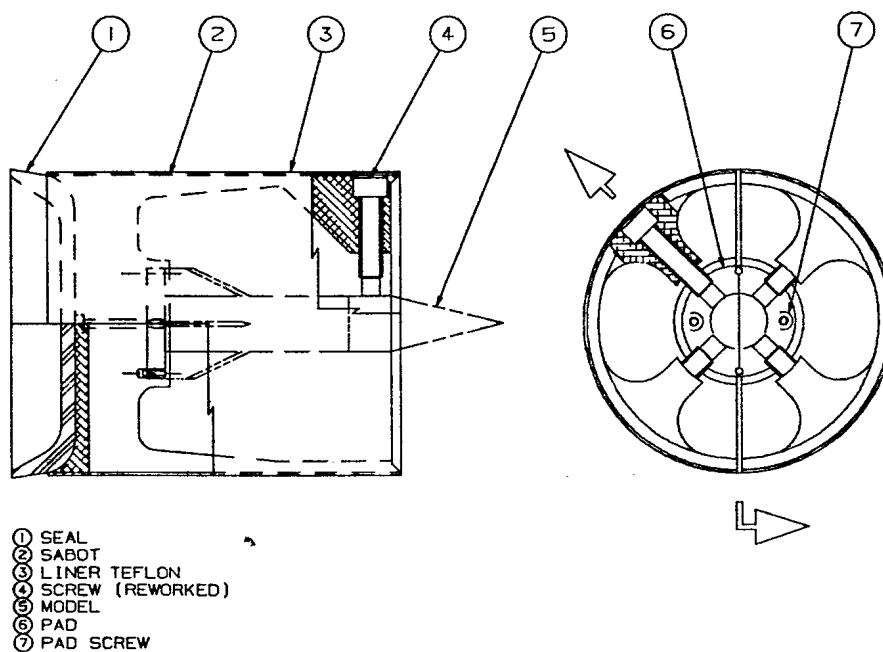
FIGURE 6 - Sabot to launch one projectile

UNCLASSIFIED

| 1 | L.15 | SEAL | 1 |
|---|------|------|---|
| 2 | ND | 1/16 TEFLON A COLLER | 1 |
| 3 | L.25 | SABOT ARRIERE | 1 |
| 4 | L.30 | SABOT AVANT | 1 |
| 5 | ND | 1/16 TEFLON COLLABLE | 1 |
| 6 | ND | PIN 1/16 ALUM | 4 |
| 7 | L.10 | VIS ASS. 6 PANS CREUX 5/16-24 | 4 |

SHEAR
PIN
(4)

.06
(TRAIT DE SCIE)

-.002
4.318
DIA.

PROFONDEUR DU TRAIT DE SCIE
APRES USINAGE DU DIA. EXT.
(TYP.)

-.05
3.8

-.05
4.0

(NE PAS ASSEMBLER)

USINER SEPAREMENT LE SABOT-AVANT ET ARRIERE
UNE FOIS LES BANDES COLLEES A LA DIMENSION
INDIQUEE.

MN
29/5/81

PROJECTILE
TANDEM

FIGURE 7 - Plan view of tandem sabot

SEAL
PAD

SABOT
(REAR)

SABOT
(FRONT)

CENTERING
SUPPORT
SCREW

DREV
MODEL
(2)
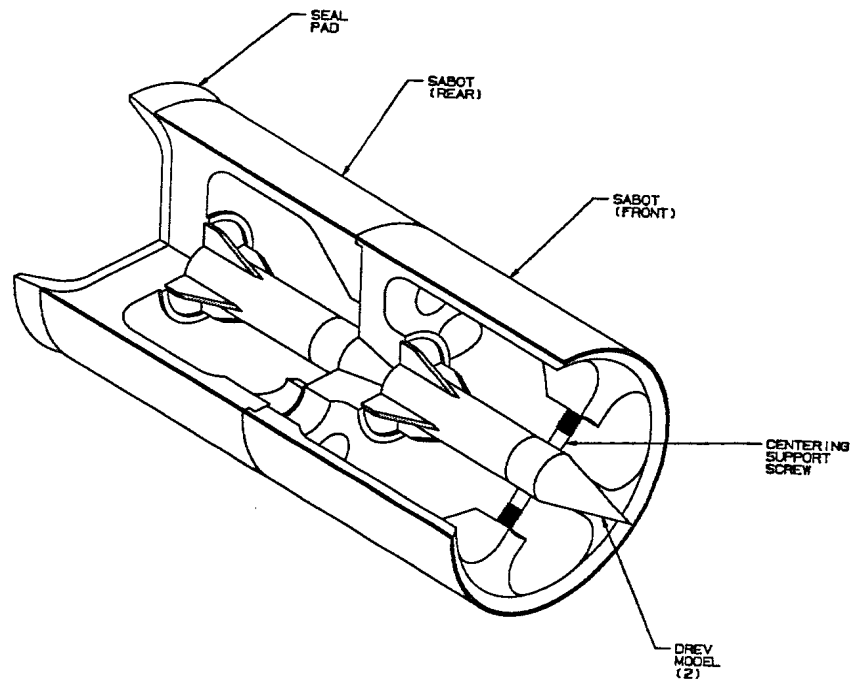
FIGURE 8 - 3 - D view of tandem sabot

UNCLASSIFIED

a)

b)
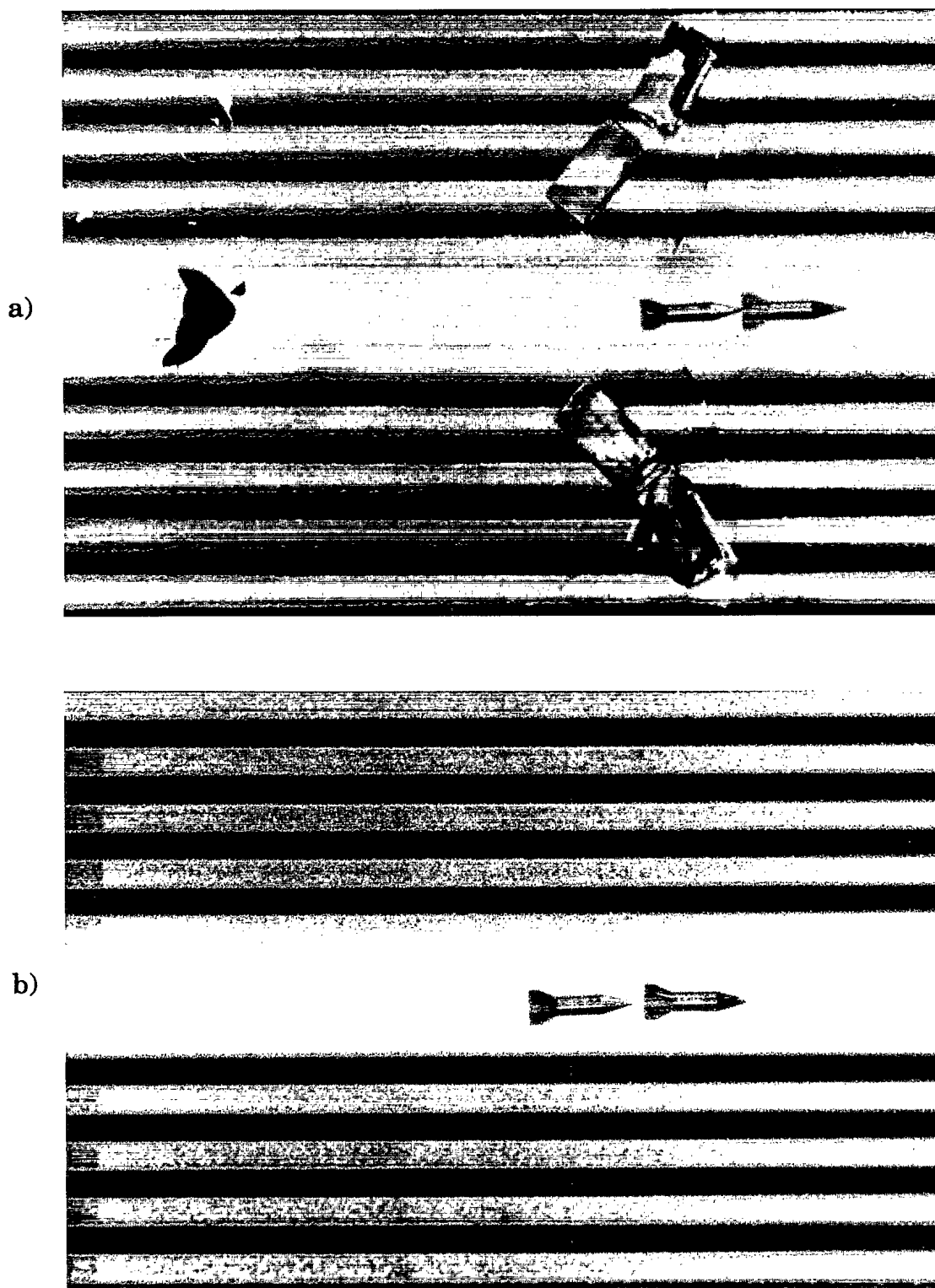
FIGURE 9    High speed camera photographs of the TD-1 shot
a) Camera - 1 - before sabot trap
b) Camera - 2 - after sabot trap
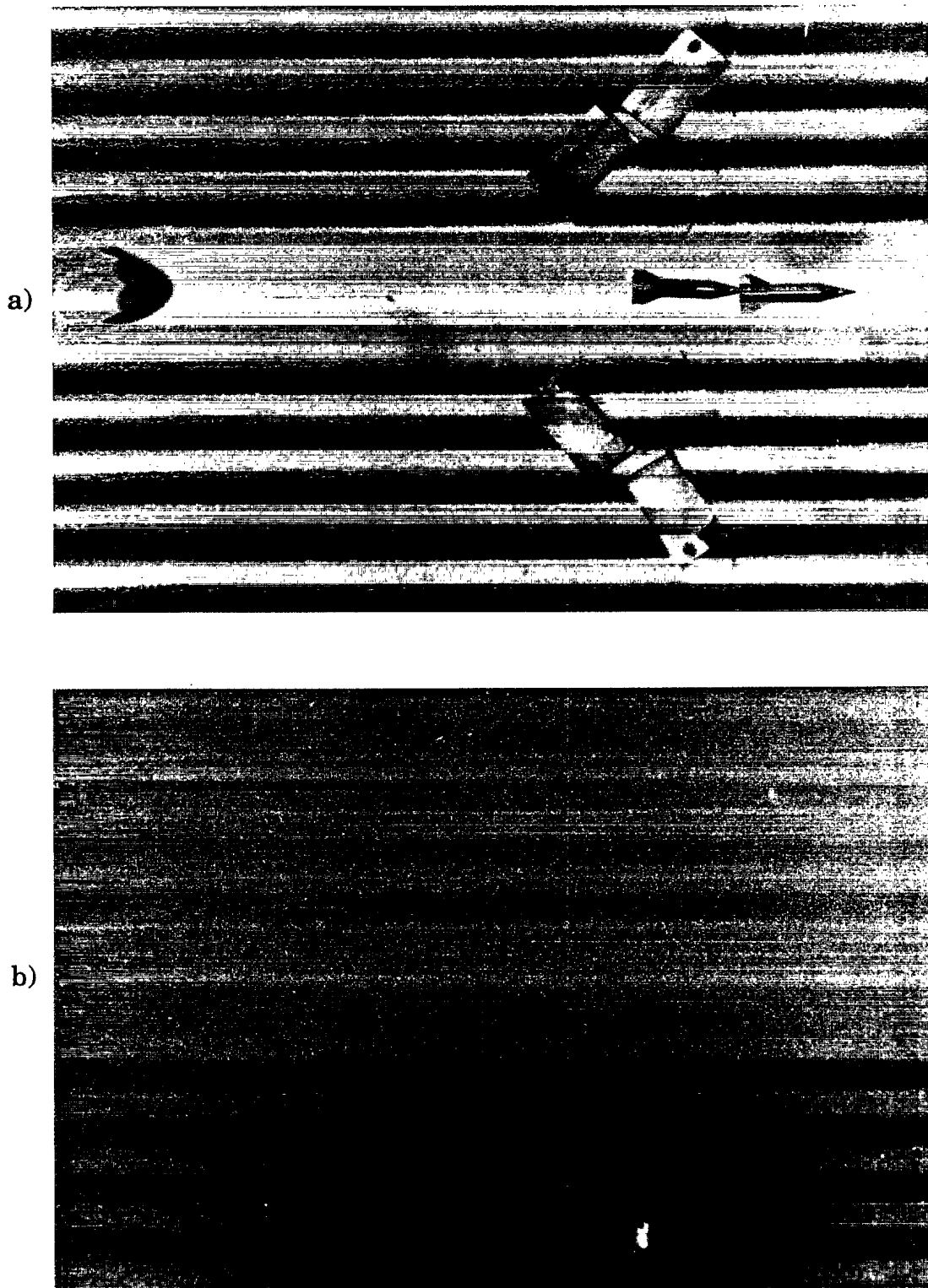
UNCLASSIFIED



FIGURE 10 High speed camera photographs of the TD-2 shot
a) Camera - 1 - before sabot trap
b) Camera - 2 - after sabot trap
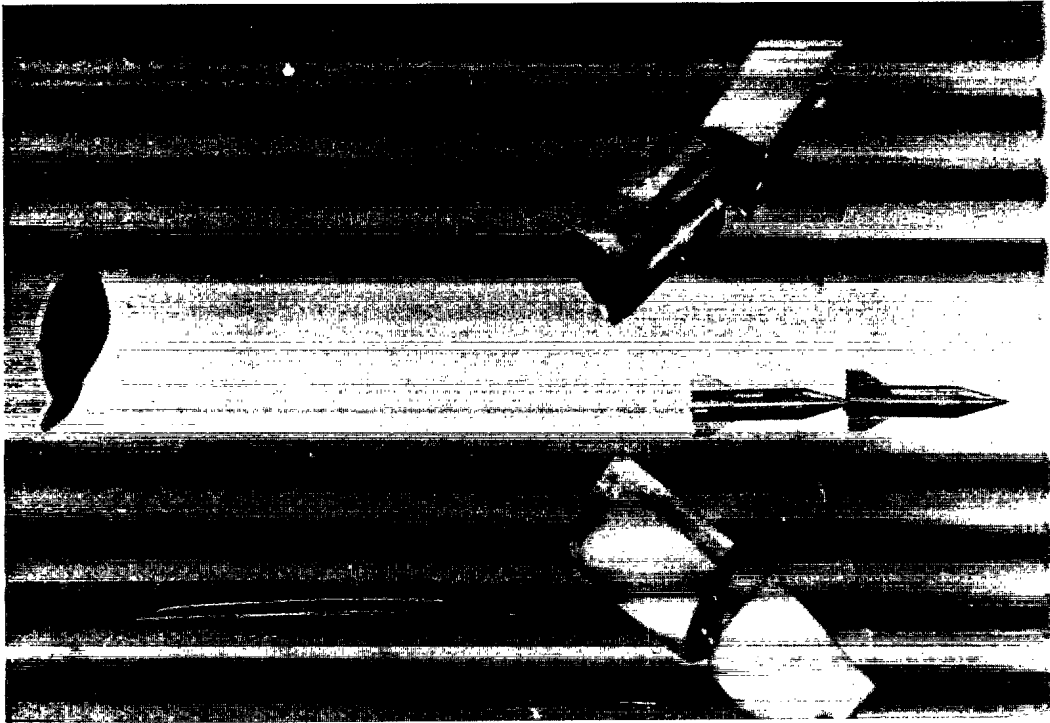
UNCLASSIFIED



FIGURE 11 High speed camera photographs of the TD-3 shot
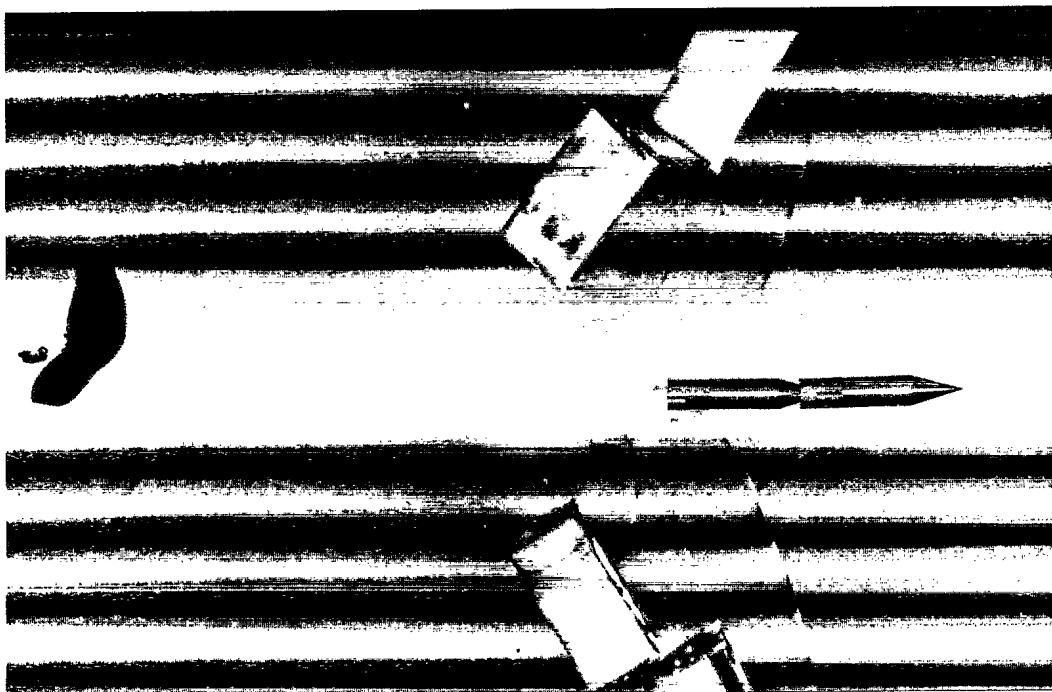


FIGURE 12 High speed camera photographs of the TD-4 shot

UNCLASSIFIED
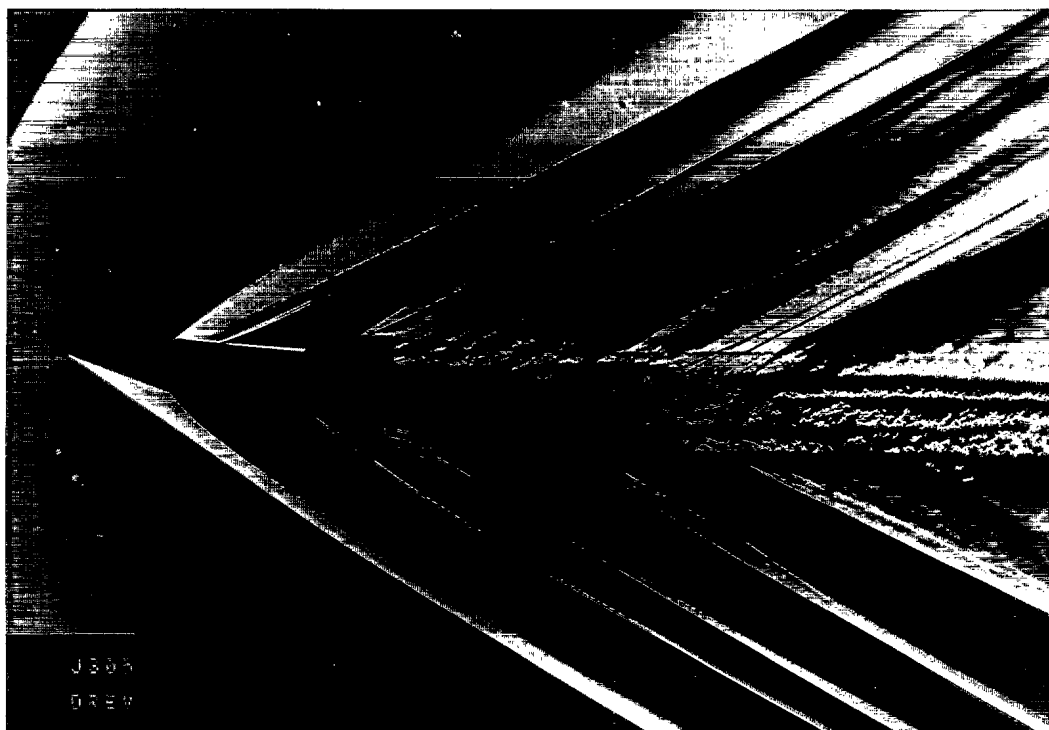


FIGURE 13 Schlieren photographs of tandem projectiles
a) Shot TD-3
b) Shot TD-4

UNCLASSIFIED
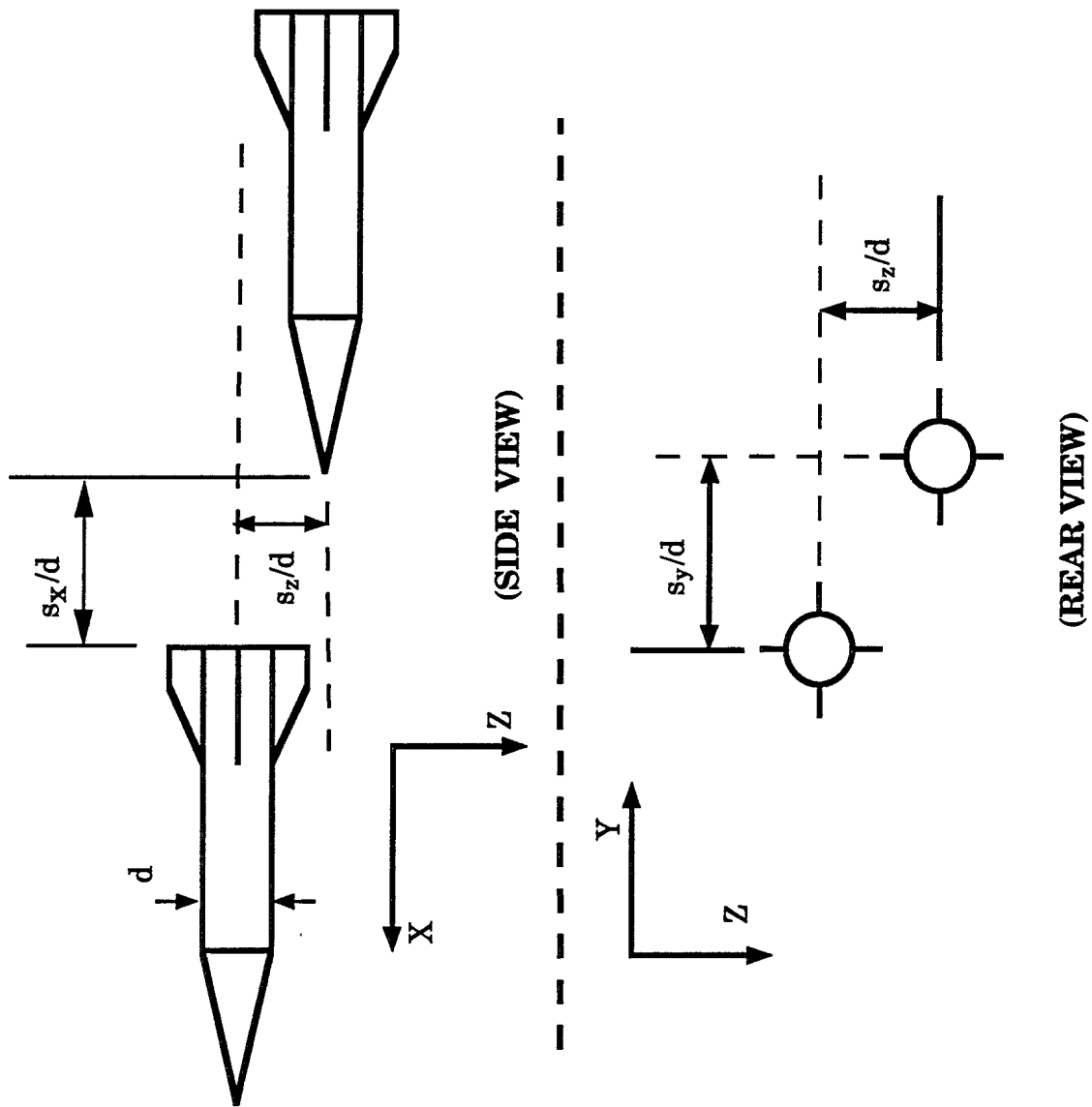


FIGURE 14  Flight terminology of tandem projectiles in flight

UNCLASSIFIED
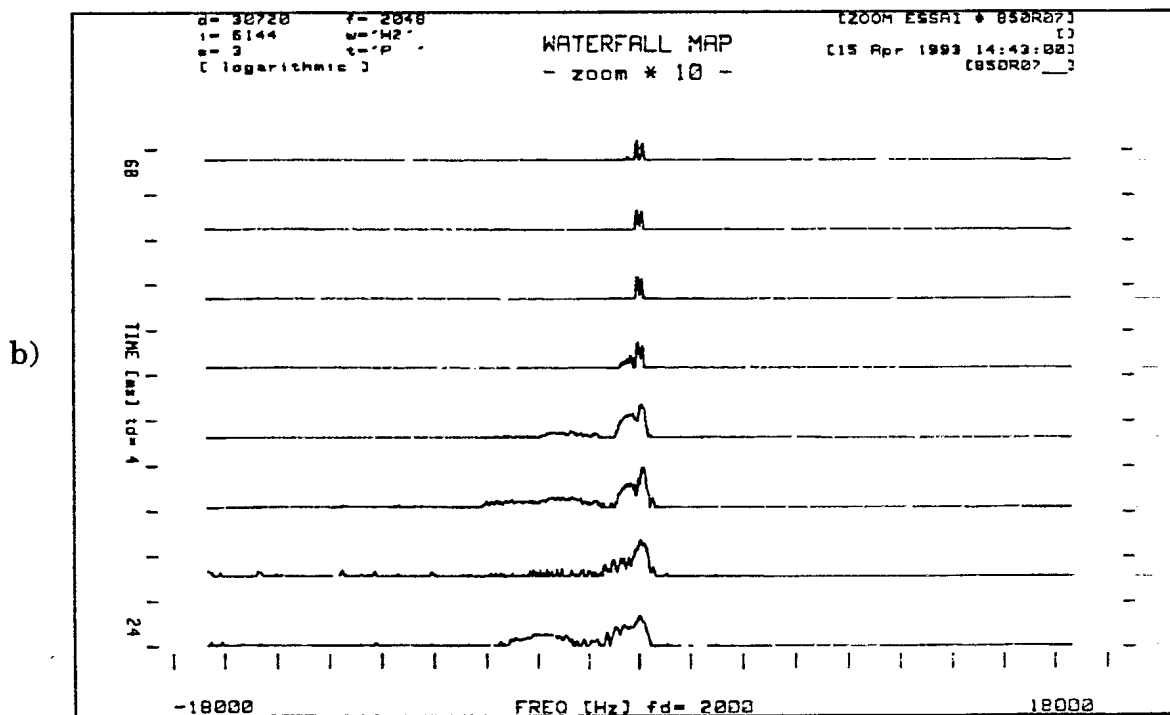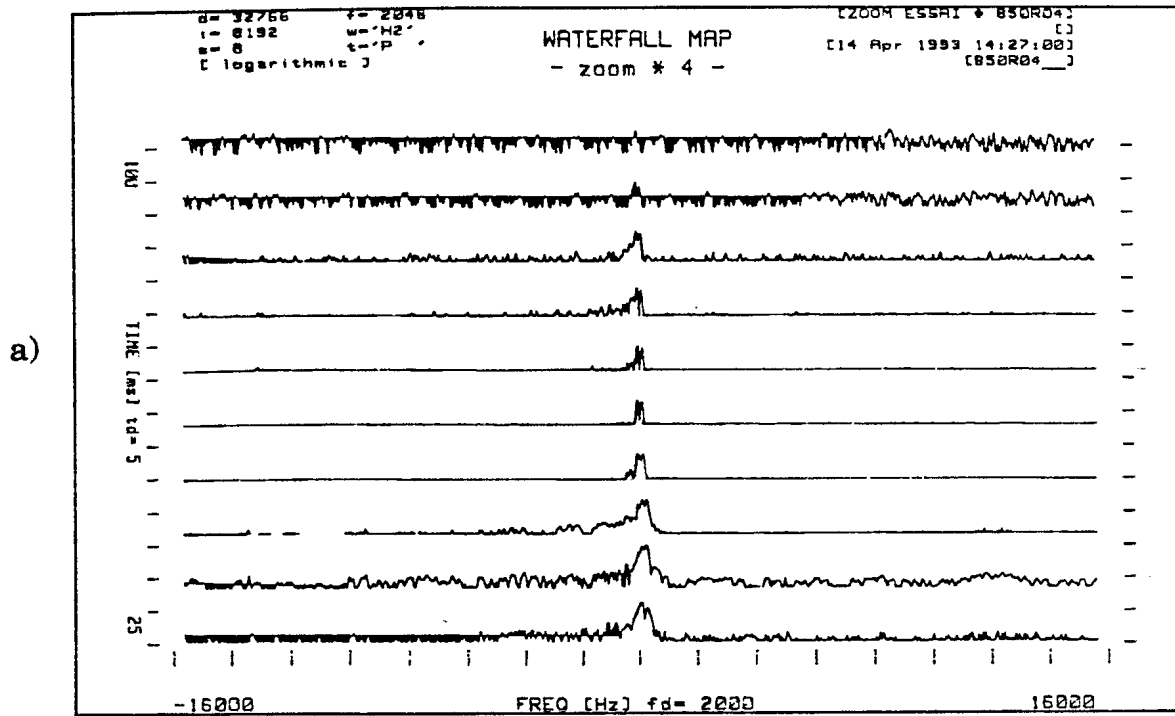


FIGURE 15 Waterfall plots
a) Shot TD-1
b) Shot TD-2

UNCLASSIFIED
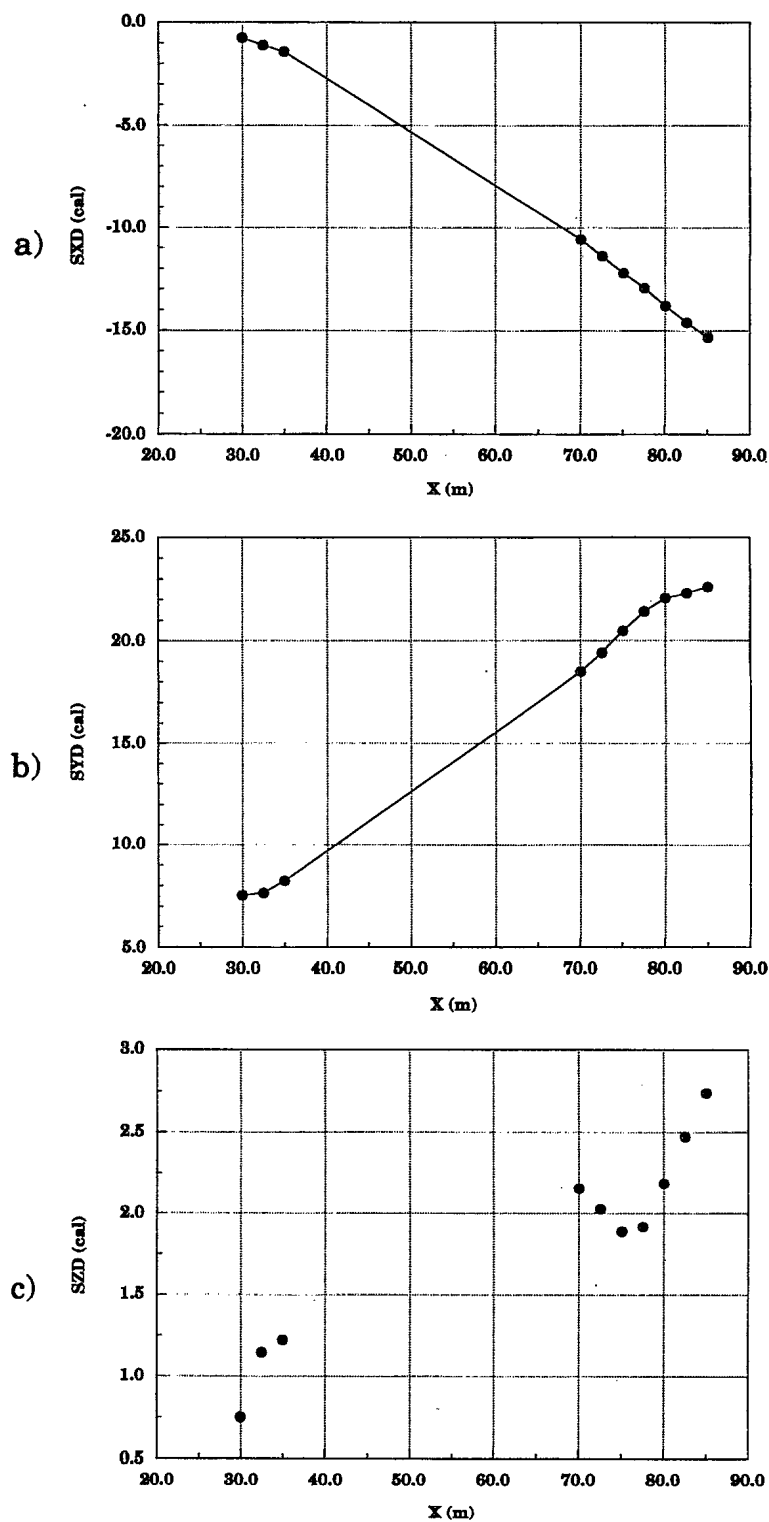


FIGURE 16  Position of second projectile relative to the first one (Shot TD-3)

a) X separation (cal)

b) Y separation (cal)

c) Z separation (cal)

UNCLASSIFIED
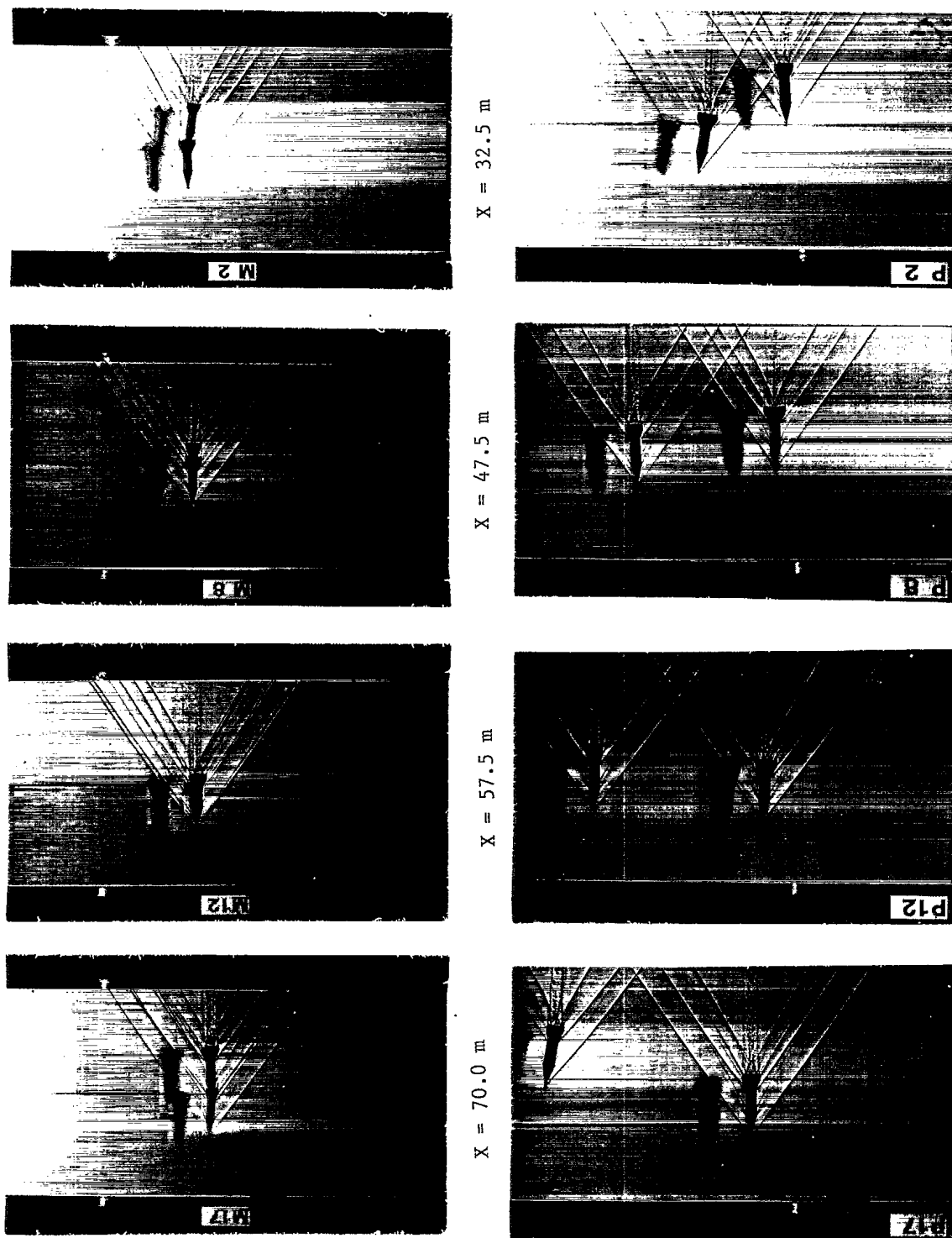


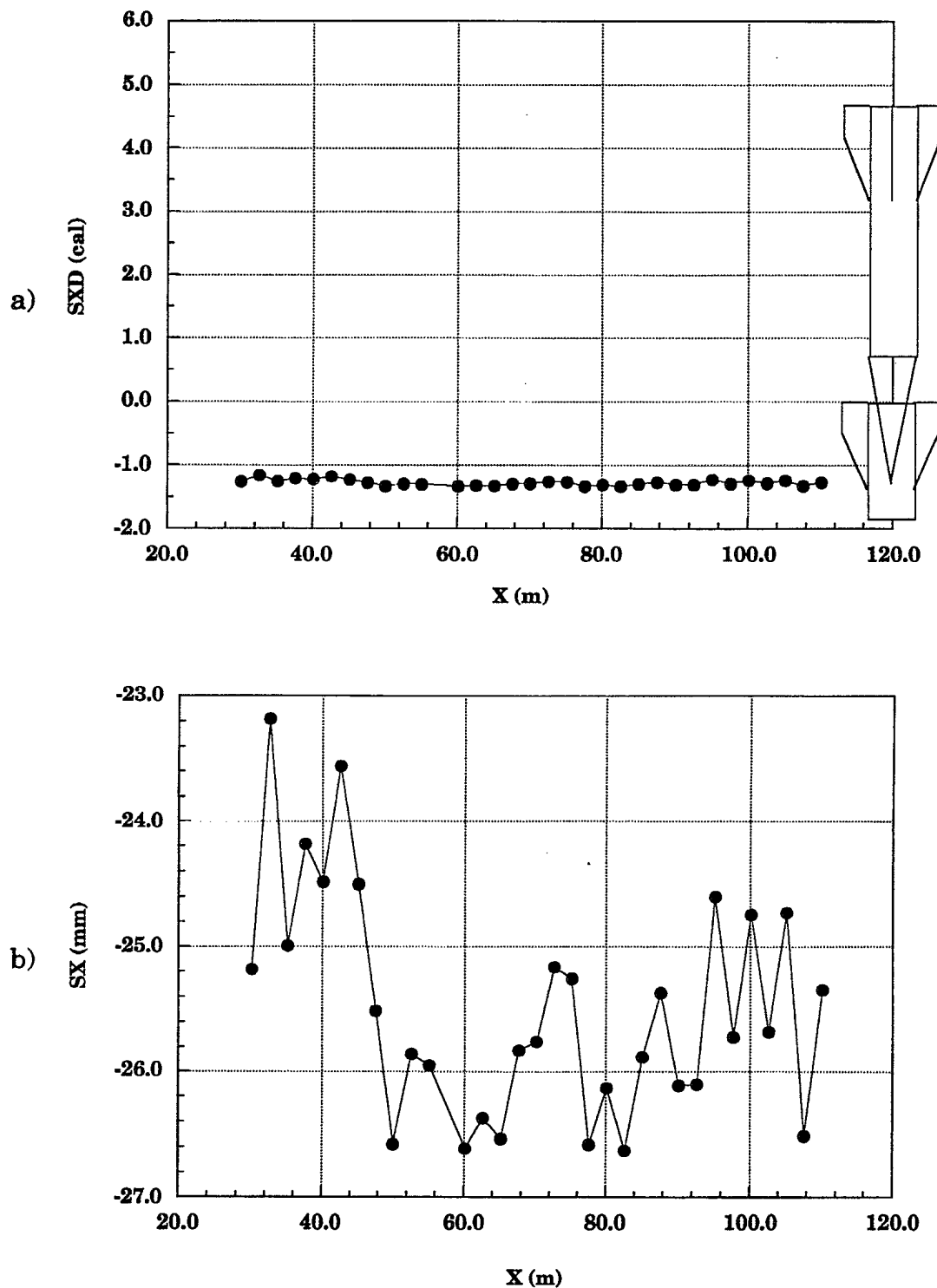FIGURE 17 Shadowgraphs of Shot TD-3

UNCLASSIFIED



FIGURE 18  Position of second projectile relative to the first one in downrange
coordinate (Shot TD-4)

a)  Overall separation view (cal)

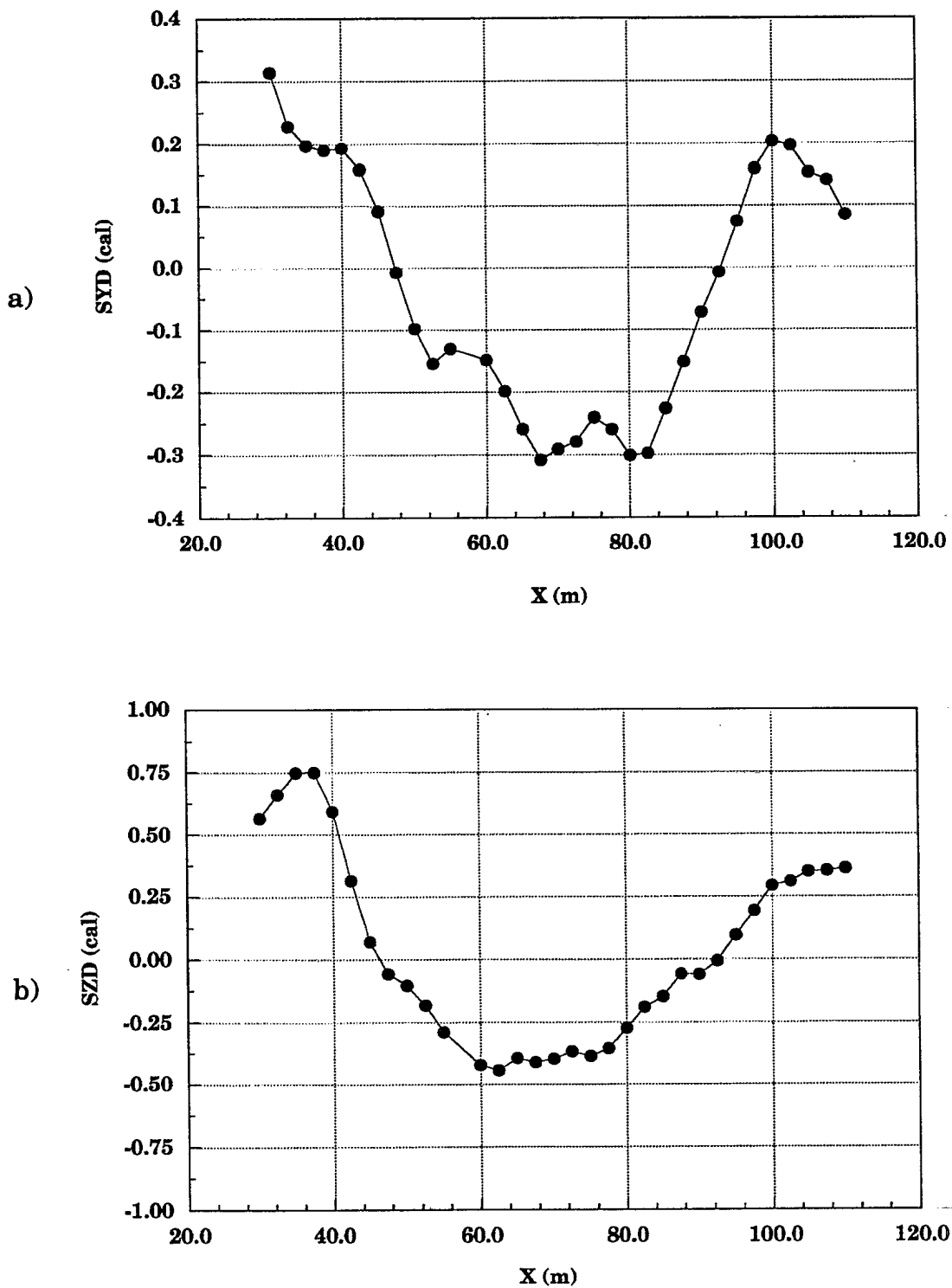b)  Expanded separation view (mm)

UNCLASSIFIED

a)



b)



FIGURE 19  Cross range position of second projectile relative to the first one
(Shot TD-4)
a) Y separation (cal)
b) Z separation (cal)
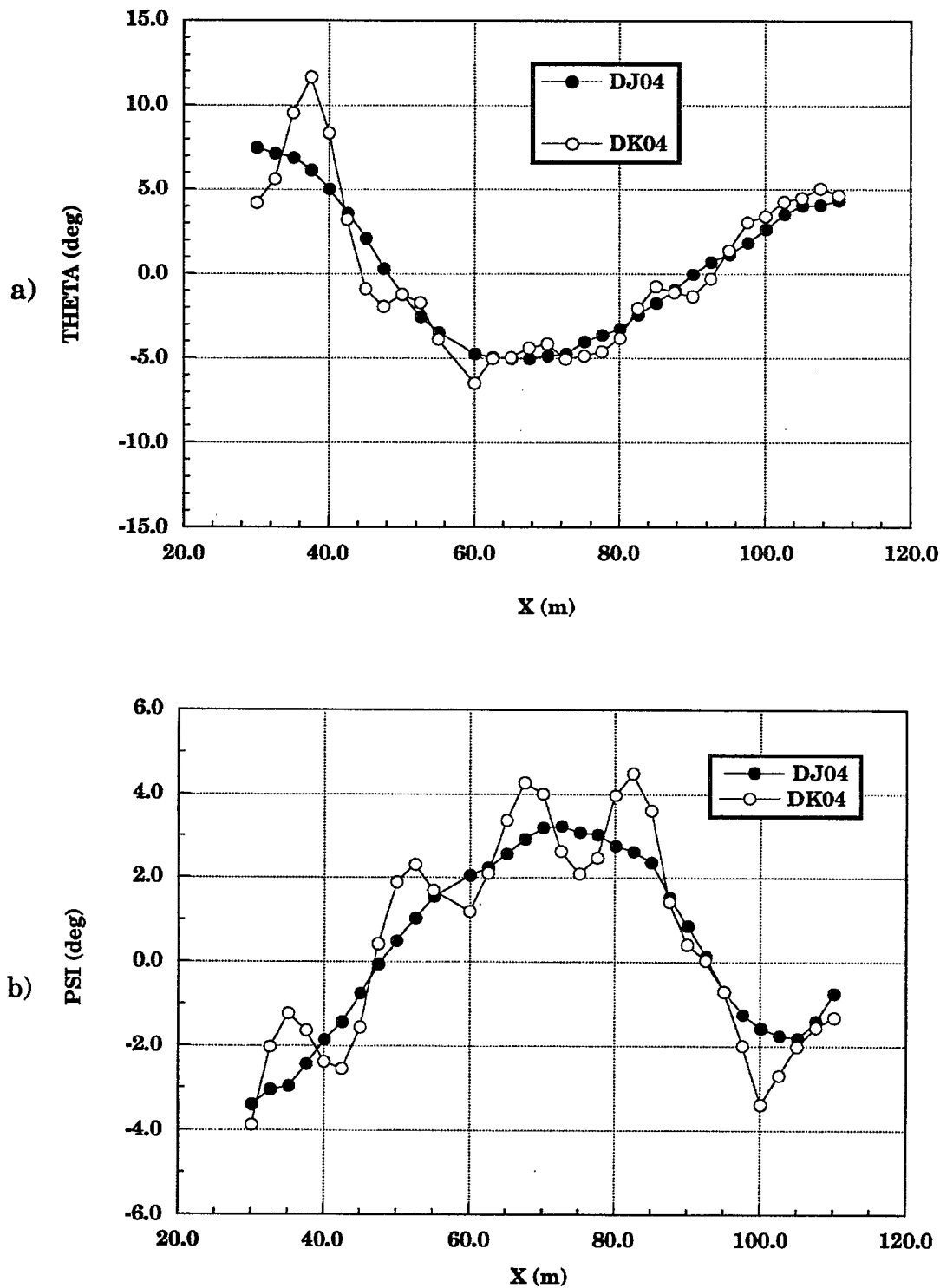
UNCLASSIFIED

a)



b)



FIGURE 20  Angular motions comparison (Shot TD-4)
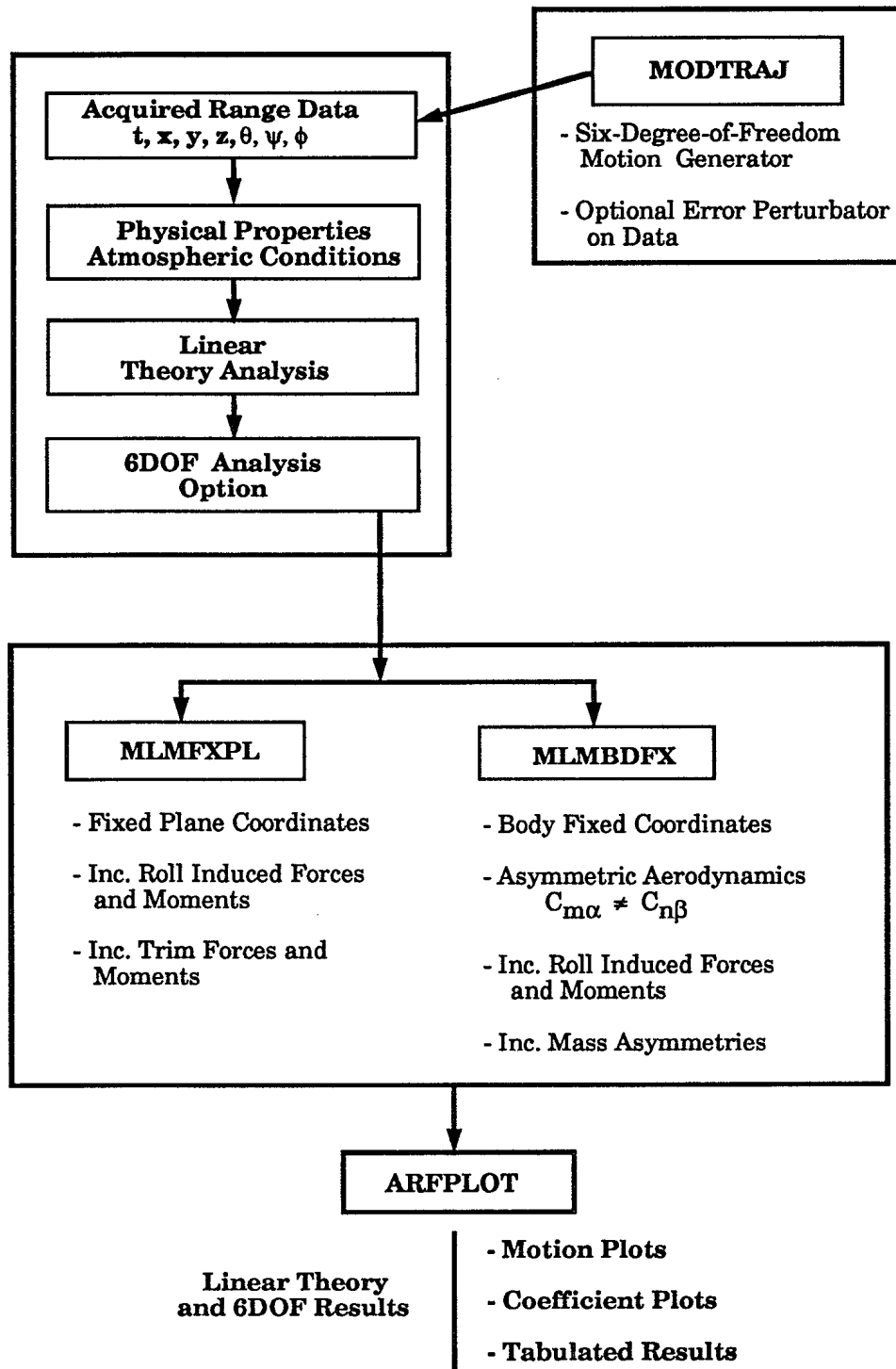a) Pitch motion
b) Yaw motion

UNCLASSIFIED



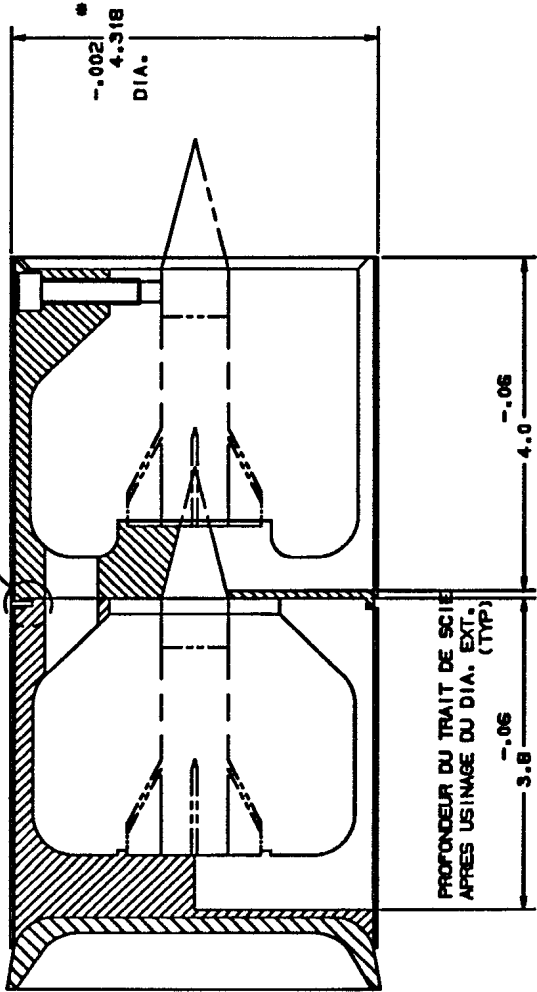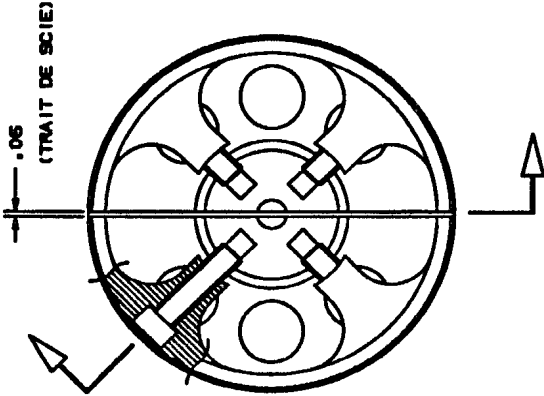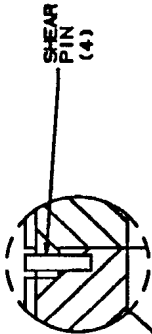FIGURE 21 - DREV Aeroballistic Range Data Analysis System (BARDAS)

ANNEX A

Detailed Drawings of Tandem Sabot Design
(Dimensions in inches)

UNCLASSIFIED
A.1

| | | |
|---|---|---|
| 1 | L15 | SEAL | 1 |
| 2 | ND | 1/16 TEFLON A COLLER | 1 |
| 3 | L25 | SABOT ARRIERE | 1 |
| 4 | L30 | SABOT AVANT | 1 |
| 5 | ND | 1/16 TEFLON COLLABLE | 1 |
| 6 | ND | PIN 1/16 ALUM | 4 |
| 7 | L10 | VIS ASS. 6 PANS CREUX 5/16-24 | 4 |

.06
(TRAIT DE SCIE)

* USINER SEPAREMENT LE SABOT-AVANT ET ARRIERE
UNE FOIS LES BANDES COLLEES A LA DIMENSION
INDIQUEE.

MN
29/5/91

PROJECTILE
TANDEM

SHEAR
PIN
(4)

*
-.002
4.318
DIA.

-.06
4.0

-.06
3.8

PROFONDEUR DU TRAIT DE SCIE
APRES USINAGE DU DIA. EXT. (TYP)

(NE PAS ASSEMBLER)

UNCLASSIFIED
A.2

MATERIEL: 75ST ALUM

6 TROUS
5/8 DIA. SUR
2.85 PC

45°     45°

4 TROUS
1/16x3/16 PROFOND
PERCER CONJ.
AVEC ITEM
(SABOT-AVANT)

SABOT-ARRIERE

-.003
4.055

2.0

+.003
.125

.188

45°

3.79

⌀.003
3.150

1.800

1.575

.060

4.27

SAND
BLAST

1/2R
TYP

.375

⌀.003
4.230
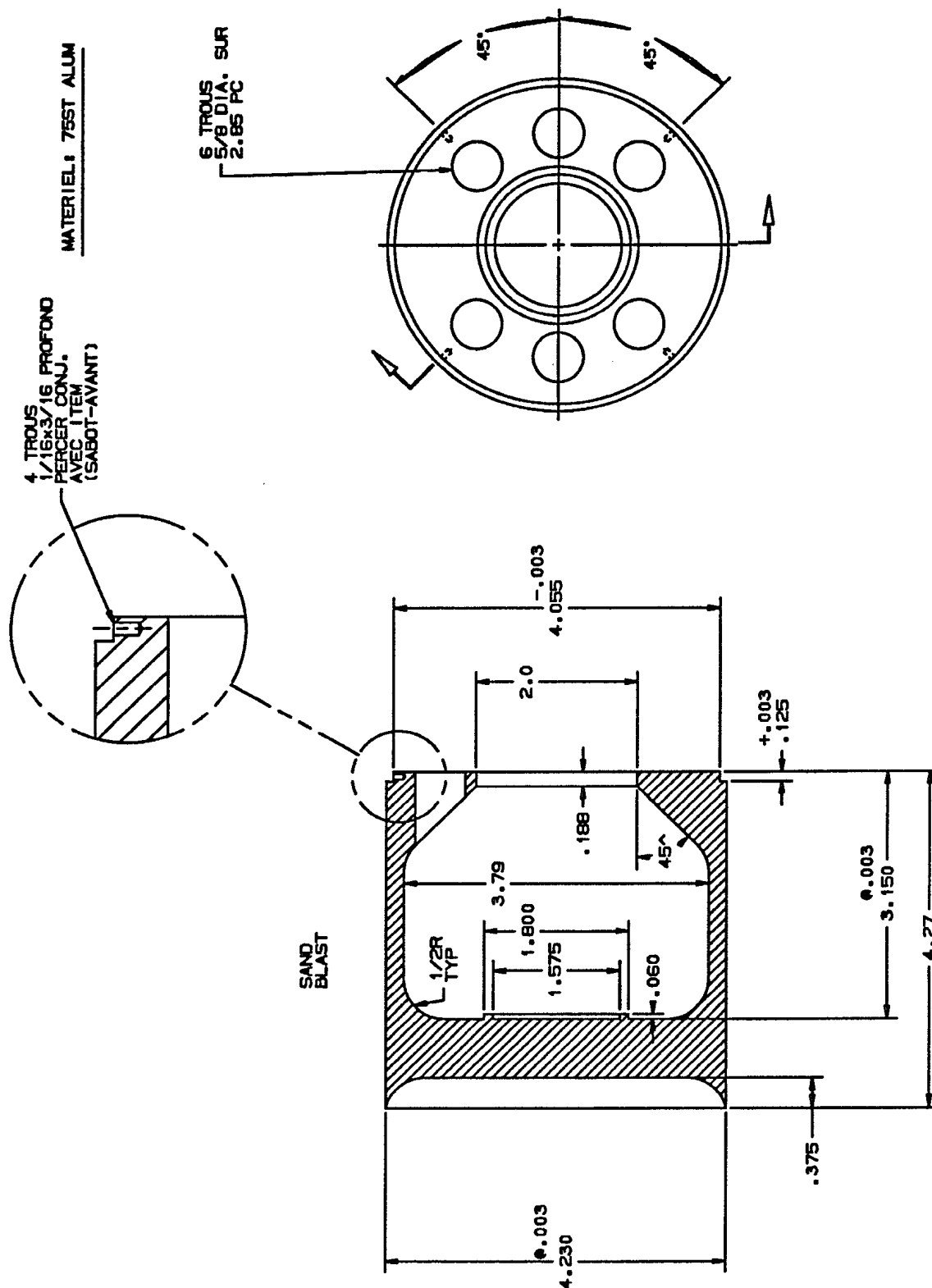
UNCLASSIFIED
A.3

SABOT—AVANT

MATERIEL: 75ST ALUM

45^

45^

45^

'1.80

'1.58

'2.00

'.50
TYP

1/2R
TYP

FORER 3/4
6 TROUS
SUR 2.85 PC

4 TROUS 1/16 DIA.
EQUIDISTANTS
PERCER CONJOINTEMENT
A L'ASSEMBLAGE
AVEC SABOT-ARRIERE

4 TROUS POUR
VA 6 PANS CREUX
5/16-24 A PROF.
INDIQUEE

SAND
BLAST

.062

45^

.41

.800

.69

.13

45^

3.86

1/2R

1/4R

.05

.44

3.96

3.65

4.28

28.1^

+.003
.787

+.003
.055

-.003
.125

+.003
4.230

4.055

UNCLASSIFIED
A.4

55°

NEOPRENE
RUBBER

R .50

4.20

4.40

.19

R .50

10°

SEAL

.88

RESURFACER

±.003
1.406

.1

.25

.25
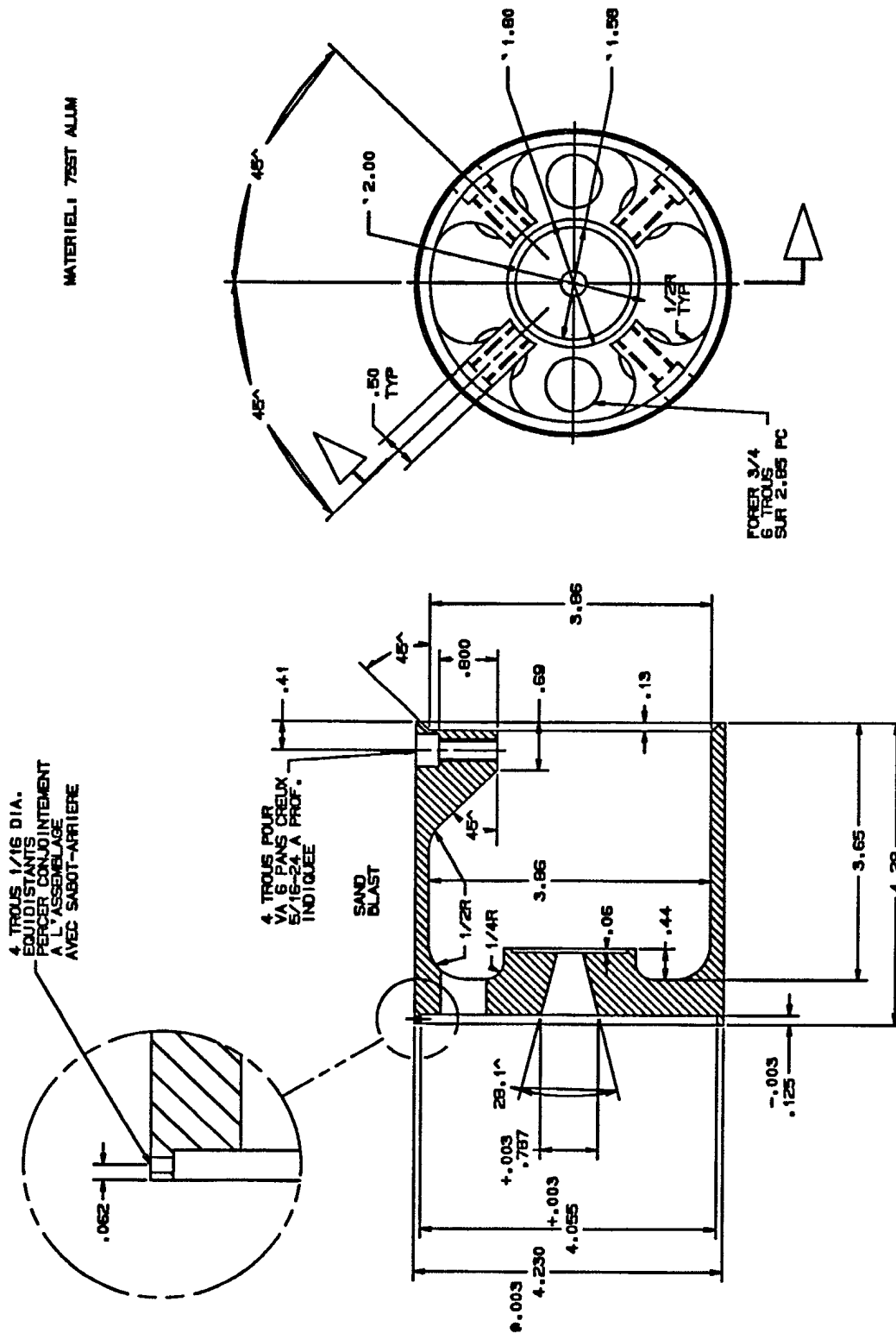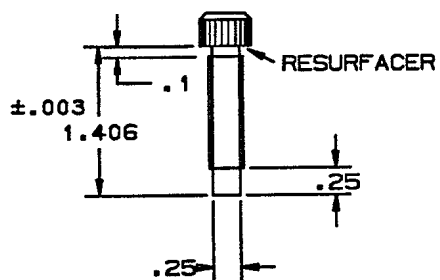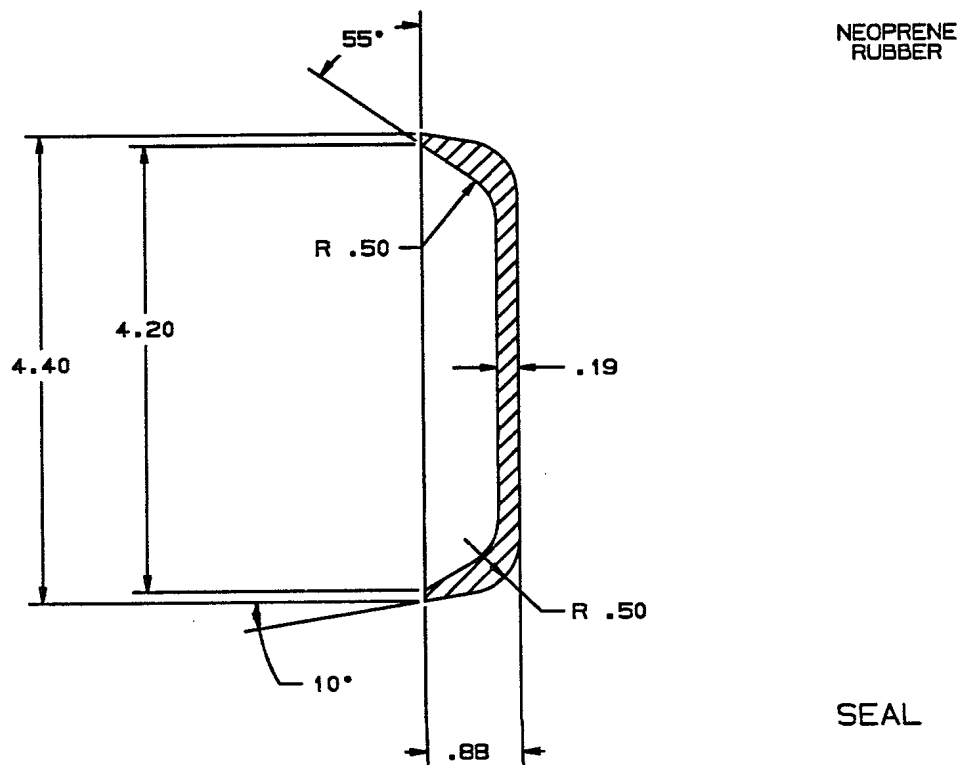
MATERIEL: VIS D'ASS.6 PANS CREUX
5/16-24 NFx1.5"LG.
(MODIFIEE)

VIS

MN
29/5/91

-.005
1.575

REAR BODY
(SUPPLIED)

Ø.002
0.787

28.1°

STRESSPROOF ST

REF
1.575

.33

2.165

1/2-28UNEF

INTERS
4.724
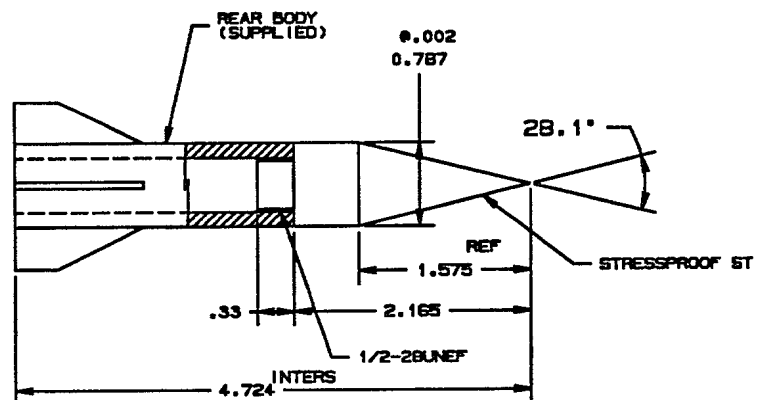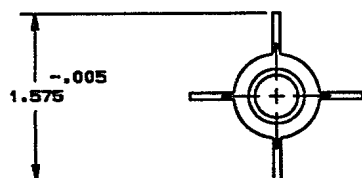
ANNEX B

Experimental Trajectory for Shot TD-3

Table BI
Experimental trajectory for Shot DJ93051303

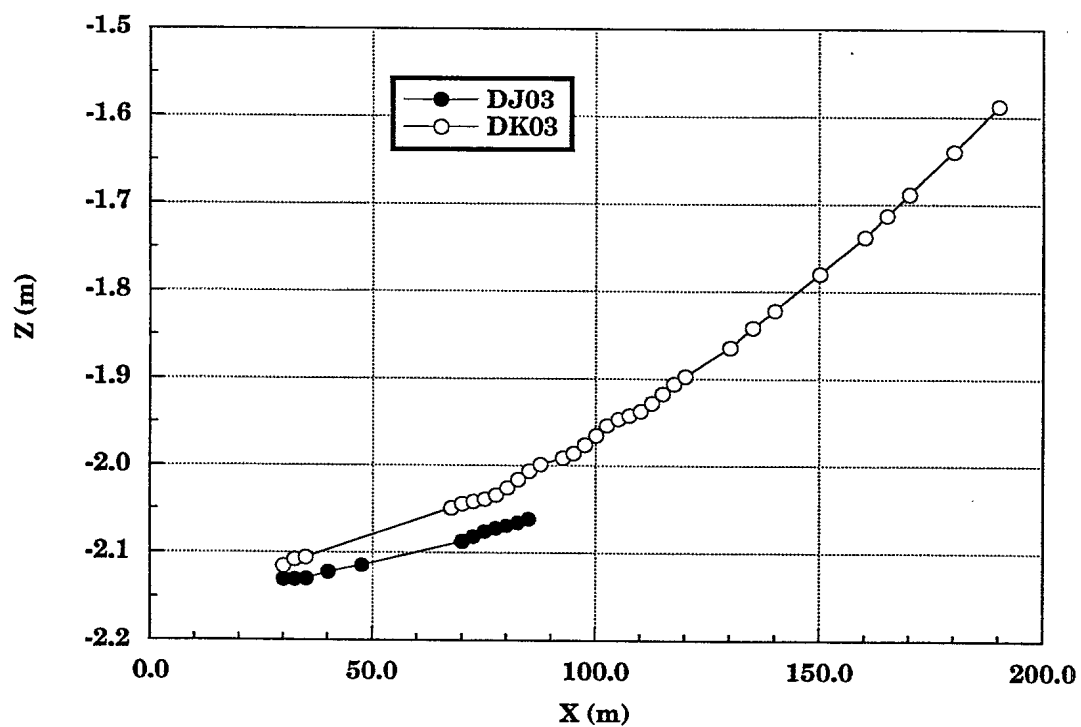| Time (s) | Y (m) | Z (m) | X (m) | θ (deg) | ψ (deg) | Window Number |
|---|---|---|---|---|---|---|
| 0.00000 | -1.65000 | -2.13040 | 30.03372 | 1.12 | 3.60 | 1 |
| 0.00373 | -1.65400 | -2.13043 | 32.53632 | -1.07 | -8.45 | 2 |
| 0.00746 | -1.66471 | -2.12992 | 35.03943 | -2.39 | -14.13 | 3 |
| 0.01492 | -1.71581 | -2.12250 | 40.02302 | 0.39 | 0.21 | 5 |
| 0.02621 | -1.77559 | -2.11447 | 47.52725 | 0.42 | 4.26 | 8 |
| 0.06034 | -1.92052 | -2.08707 | 69.95024 | -0.94 | -9.27 | 17 |
| 0.06414 | -1.94037 | -2.08188 | 72.42722 | -0.66 | -6.40 | 18 |
| 0.06797 | -1.96607 | -2.07604 | 74.91347 | 0.69 | 1.19 | 19 |
| 0.07179 | -1.98861 | -2.07193 | 77.39838 | 1.13 | 7.07 | 20 |
| 0.07563 | -2.00871 | -2.06898 | 79.88506 | 0.60 | 7.33 | 21 |
| 0.07945 | -2.01972 | -2.06526 | 82.35681 | -0.59 | 1.28 | 22 |
| 0.08330 | -2.03006 | -2.06108 | 84.84444 | -1.19 | -5.36 | 23 |

Table BII
Experimental trajectory for Shot DK93051303

| Time (s) | Y (m) | Z (m) | X (m) | θ (deg) | ψ (deg) | Window Number |
|---|---|---|---|---|---|---|
| 0.00000 | -1.49909 | -2.11539 | 29.92872 | 4.05 | 3.28 | 1 |
| 0.00373 | -1.50098 | -2.10750 | 32.43846 | 6.51 | 3.22 | 2 |
| 0.00746 | -1.50029 | -2.10548 | 34.94772 | 4.77 | -0.19 | 3 |
| 0.05653 | -1.54727 | -2.04905 | 67.54246 | 4.85 | 1.63 | 16 |
| 0.06034 | -1.55026 | -2.04397 | 70.04195 | 3.82 | -0.26 | 17 |
| 0.06414 | -1.55189 | -2.04134 | 72.53516 | 0.36 | -1.88 | 18 |
| 0.06796 | -1.55630 | -2.03828 | 75.03811 | -2.88 | -2.16 | 19 |
| 0.07179 | -1.56003 | -2.03361 | 77.53759 | -4.28 | -0.97 | 20 |
| 0.07563 | -1.56729 | -2.02524 | 80.04160 | -2.74 | 0.71 | 21 |
| 0.07945 | -1.57359 | -2.01584 | 82.52944 | 0.51 | 1.95 | 22 |
| 0.08330 | -1.57770 | -2.00628 | 85.03106 | 3.00 | 1.32 | 23 |
| 0.08715 | -1.57960 | -1.99860 | 87.52937 | 3.27 | 0.30 | 24 |
| 0.09486 | -1.58576 | -1.99118 | 92.52189 | -2.60 | -2.05 | 26 |
| 0.09873 | -1.59126 | -1.98547 | 95.02188 | -4.58 | -0.81 | 27 |
| 0.10262 | -1.59783 | -1.97606 | 97.52708 | -2.97 | 1.38 | 28 |
| 0.10650 | -1.60258 | -1.96478 | 100.02248 | 1.27 | 2.34 | 29 |
| 0.11038 | -1.60561 | -1.95349 | 102.52104 | 4.25 | 0.66 | 30 |
| 0.11429 | -1.60737 | -1.94628 | 105.02568 | 3.10 | -1.74 | 31 |
| 0.11817 | -1.61155 | -1.94203 | 107.51202 | -0.57 | -2.30 | 32 |
| 0.12209 | -1.61770 | -1.93711 | 110.01916 | -3.95 | -0.11 | 33 |
| 0.12601 | -1.62397 | -1.92776 | 112.52304 | -3.39 | 1.94 | 34 |
| 0.12993 | -1.62746 | -1.91697 | 115.01911 | -0.47 | 1.97 | 35 |
| 0.13385 | -1.63027 | -1.90568 | 117.51104 | 2.03 | -0.18 | 36 |
| 0.13780 | -1.63337 | -1.89702 | 120.01486 | 2.14 | -1.88 | 37 |
| 0.15360 | -1.65237 | -1.86371 | 130.01369 | -1.21 | 1.03 | 41 |
| 0.16157 | -1.65922 | -1.84142 | 135.02693 | 0.53 | -0.57 | 43 |
| 0.16951 | -1.66699 | -1.82160 | 140.01016 | 0.40 | -1.12 | 45 |
| 0.18554 | -1.68499 | -1.77973 | 150.02074 | 1.07 | -0.04 | 49 |
| 0.20168 | -1.70336 | -1.73767 | 160.02890 | -0.95 | 1.49 | 53 |
| 0.20976 | -1.71021 | -1.71292 | 165.01578 | 0.26 | -0.21 | 55 |
| 0.21790 | -1.71751 | -1.68815 | 170.02473 | -0.30 | -0.84 | 57 |
| 0.23420 | -1.73661 | -1.63926 | 180.00777 | 0.18 | 0.80 | 61 |
| 0.25067 | -1.75247 | -1.58749 | 190.02609 | -0.64 | -0.09 | 65 |

UNCLASSIFIED
B.1
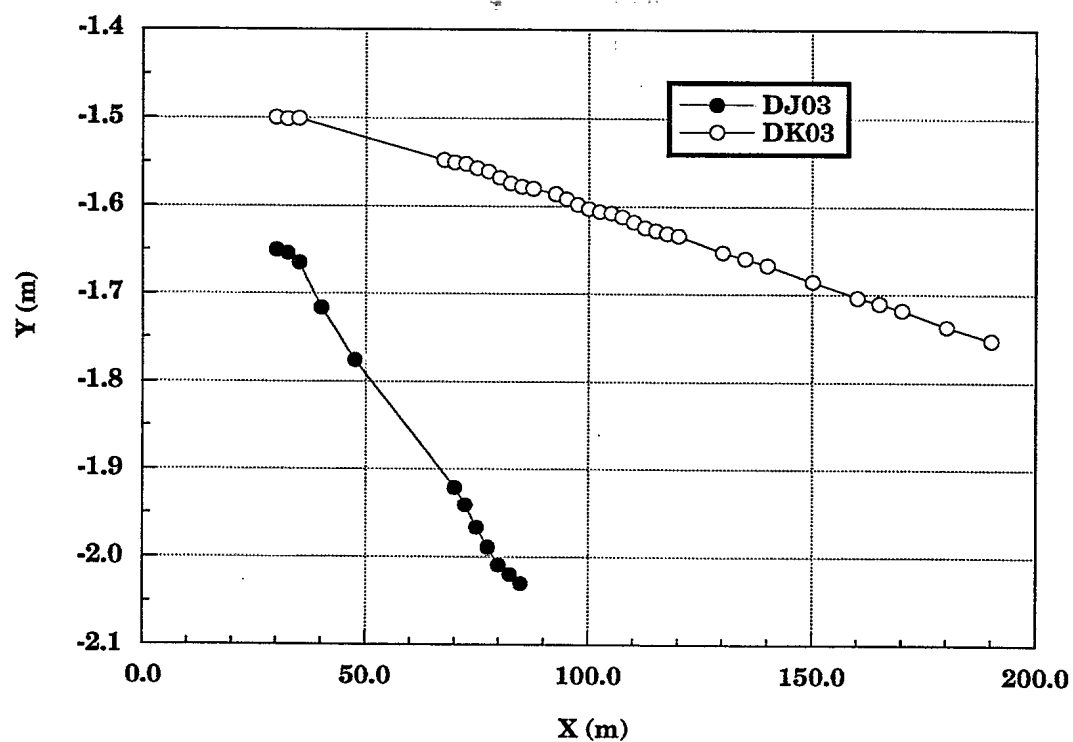
UNCLASSIFIED
B.2
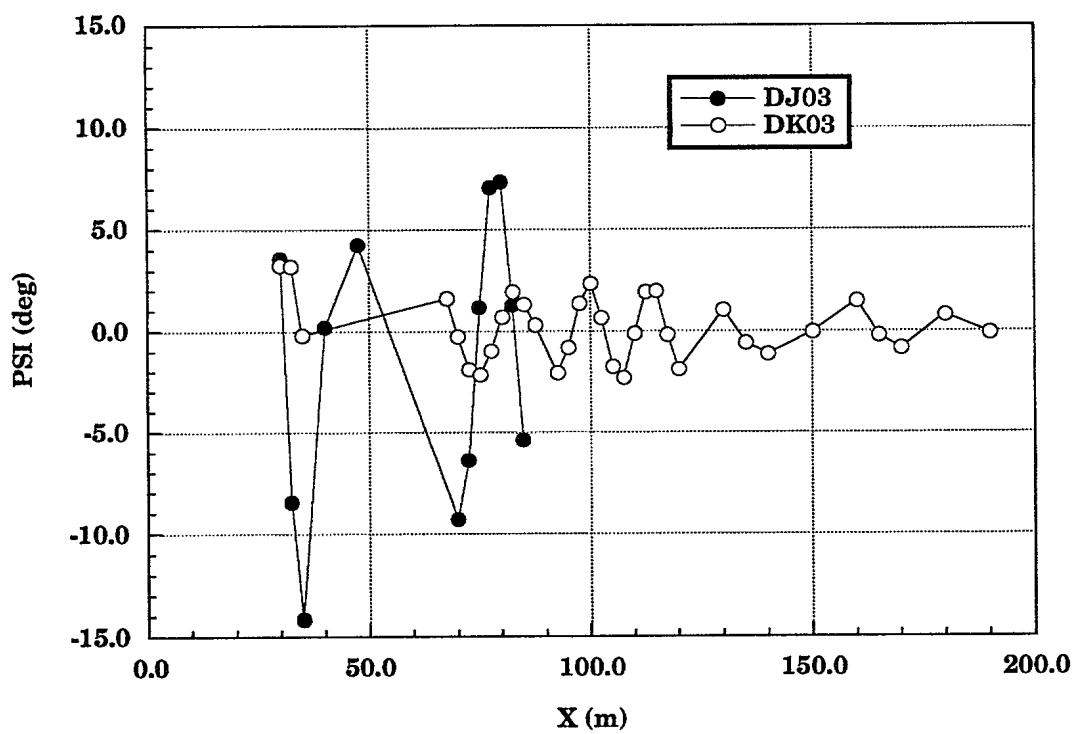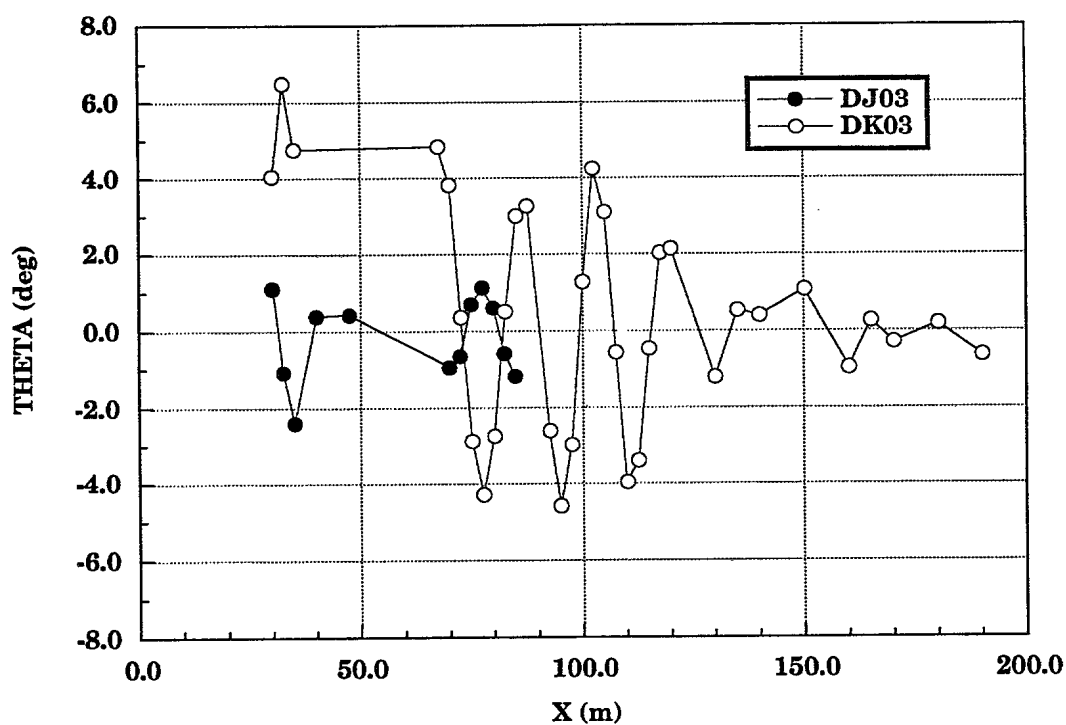
# ANNEX C

## Experimental Trajectory for Shot TD-4

Table CI
Experimental trajectory for Shot DJ93051304

| Time (s) | Y (m) | Z (m) | X (m) | θ (deg) | ψ (deg) | Window Number |
|---|---|---|---|---|---|---|
| 0.00000 | -1.54709 | -2.28658 | 30.12190 | 7.50 | -3.40 | 1 |
| 0.00367 | -1.56004 | -2.31973 | 32.62675 | 7.16 | -3.05 | 2 |
| 0.00734 | -1.57479 | -2.35676 | 35.12915 | 6.92 | -2.95 | 3 |
| 0.01101 | -1.59085 | -2.39681 | 37.62640 | 6.16 | -2.43 | 4 |
| 0.01467 | -1.60849 | -2.44033 | 40.11723 | 5.03 | -1.85 | 5 |
| 0.01834 | -1.62716 | -2.48620 | 42.61546 | 3.58 | -1.43 | 6 |
| 0.02204 | -1.64640 | -2.53439 | 45.12219 | 2.12 | -0.75 | 7 |
| 0.02572 | -1.66591 | -2.58212 | 47.61098 | 0.30 | -0.05 | 8 |
| 0.02940 | -1.68464 | -2.62904 | 50.10693 | -1.24 | 0.50 | 9 |
| 0.03311 | -1.70255 | -2.67458 | 52.61533 | -2.54 | 1.03 | 10 |
| 0.03681 | -1.72061 | -2.71787 | 55.11697 | -3.46 | 1.55 | 11 |
| 0.04422 | -1.75117 | -2.79523 | 60.11033 | -4.75 | 2.05 | 13 |
| 0.04793 | -1.76409 | -2.82808 | 62.60858 | -4.94 | 2.23 | 14 |
| 0.05165 | -1.77440 | -2.85764 | 65.11450 | -5.02 | 2.57 | 15 |
| 0.05539 | -1.78314 | -2.88430 | 67.62336 | -5.03 | 2.92 | 16 |
| 0.05911 | -1.79090 | -2.90645 | 70.11736 | -4.86 | 3.20 | 17 |
| 0.06284 | -1.79606 | -2.92507 | 72.61900 | -4.73 | 3.23 | 18 |
| 0.06658 | -1.79954 | -2.93975 | 75.12352 | -4.03 | 3.08 | 19 |
| 0.07032 | -1.79922 | -2.95253 | 77.61879 | -3.62 | 3.03 | 20 |
| 0.07406 | -1.79837 | -2.96273 | 80.12051 | -3.26 | 2.76 | 21 |
| 0.07781 | -1.79651 | -2.97054 | 82.61639 | -2.42 | 2.63 | 22 |
| 0.08157 | -1.79222 | -2.97545 | 85.11897 | -1.72 | 2.36 | 23 |
| 0.08533 | -1.78483 | -2.98146 | 87.62185 | -0.96 | 1.53 | 24 |
| 0.08909 | -1.77843 | -2.98499 | 90.12285 | -0.03 | 0.85 | 25 |
| 0.09285 | -1.77093 | -2.98855 | 92.61791 | 0.71 | 0.14 | 26 |
| 0.09661 | -1.76331 | -2.99245 | 95.11813 | 1.17 | -0.71 | 27 |
| 0.10040 | -1.75742 | -2.99644 | 97.62860 | 1.86 | -1.25 | 28 |
| 0.10417 | -1.75166 | -3.00179 | 100.1251 | 2.64 | -1.57 | 29 |
| 0.10794 | -1.74688 | -3.00823 | 102.6207 | 3.51 | -1.74 | 30 |
| 0.11174 | -1.74388 | -3.01693 | 105.1263 | 4.04 | -1.81 | 31 |
| 0.11552 | -1.74199 | -3.02740 | 107.6196 | 4.09 | -1.40 | 32 |
| 0.11931 | -1.74038 | -3.04055 | 110.1231 | 4.35 | -0.74 | 33 |

Table CII
Experimental trajectory for Shot DK93051304

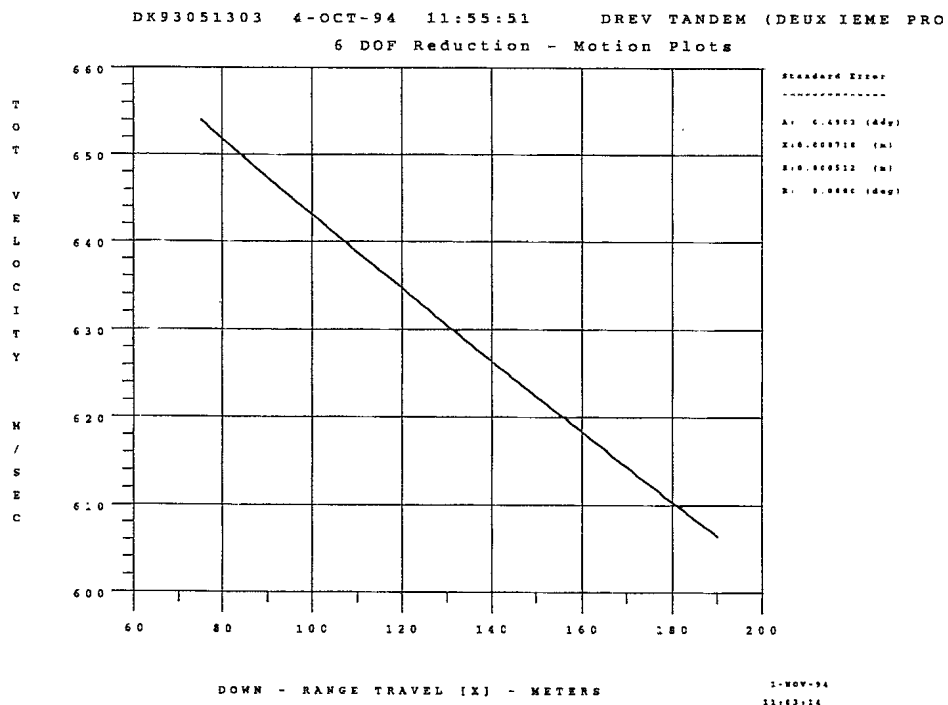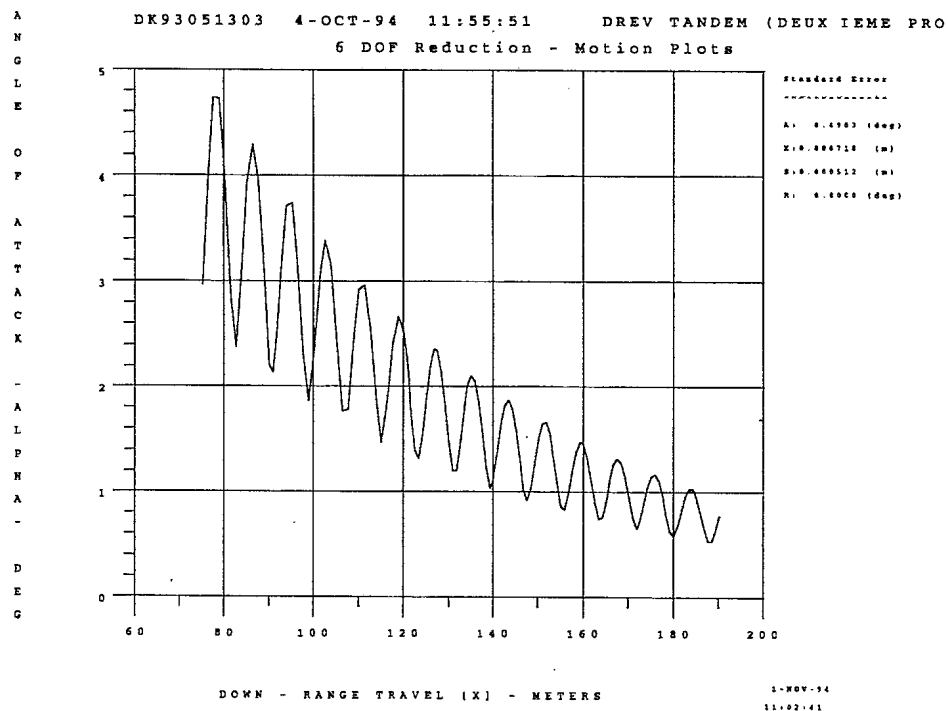| Time (s) | Y (m) | Z (m) | X (m) | θ (deg) | ψ (deg) | Window Number |
|---|---|---|---|---|---|---|
| 0.00000 | -1.54077 | -2.27533 | 30.02701 | 4.22 | -3.87 | 1 |
| 0.00367 | -1.55547 | -2.30652 | 32.52975 | 5.63 | -2.02 | 2 |
| 0.00734 | -1.57084 | -2.34178 | 35.03396 | 9.58 | -1.23 | 3 |
| 0.01101 | -1.58704 | -2.38179 | 37.53040 | 11.67 | -1.62 | 4 |
| 0.01467 | -1.60462 | -2.42847 | 40.02153 | 8.37 | -2.38 | 5 |
| 0.01834 | -1.62398 | -2.47989 | 42.51884 | 3.23 | -2.54 | 6 |
| 0.02204 | -1.64456 | -2.53296 | 45.02651 | -0.90 | -1.56 | 7 |
| 0.02572 | -1.66604 | -2.58327 | 47.51631 | -1.94 | 0.42 | 8 |
| 0.02940 | -1.68658 | -2.63111 | 50.01333 | -1.22 | 1.89 | 9 |
| 0.03311 | -1.70561 | -2.67822 | 52.52101 | -1.70 | 2.31 | 10 |
| 0.03681 | -1.72320 | -2.72362 | 55.02274 | -3.89 | 1.69 | 11 |
| 0.04422 | -1.75411 | -2.80365 | 60.01676 | -6.48 | 1.20 | 13 |
| 0.04793 | -1.76805 | -2.83694 | 62.51477 | -5.03 | 2.10 | 14 |
| 0.05165 | -1.77957 | -2.86549 | 65.02086 | -4.94 | 3.37 | 15 |
| 0.05539 | -1.78930 | -2.89251 | 67.52901 | -4.39 | 4.28 | 16 |
| 0.05911 | -1.79671 | -2.91437 | 70.02294 | -4.15 | 4.02 | 17 |
| 0.06284 | -1.80163 | -2.93241 | 72.52399 | -5.05 | 2.63 | 18 |
| 0.06658 | -1.80434 | -2.94747 | 75.02859 | -4.86 | 2.09 | 19 |
| 0.07032 | -1.80440 | -2.95962 | 77.52519 | -4.61 | 2.48 | 20 |
| 0.07406 | -1.80438 | -2.96819 | 80.02647 | -3.81 | 3.98 | 21 |
| 0.07781 | -1.80246 | -2.97433 | 82.52284 | -2.03 | 4.50 | 22 |
| 0.08157 | -1.79674 | -2.97841 | 85.02467 | -0.76 | 3.61 | 23 |
| 0.08533 | -1.78784 | -2.98262 | 87.52704 | -1.10 | 1.42 | 24 |
| 0.08909 | -1.77986 | -2.98619 | 90.02878 | -1.33 | 0.42 | 25 |
| 0.09285 | -1.77106 | -2.98867 | 92.52383 | -0.30 | 0.04 | 26 |
| 0.09661 | -1.76180 | -2.99049 | 95.02254 | 1.40 | -0.70 | 27 |
| 0.10040 | -1.75423 | -2.99255 | 97.53414 | 3.05 | -1.99 | 28 |
| 0.10417 | -1.74758 | -2.99591 | 100.0296 | 3.42 | -3.39 | 29 |
| 0.10794 | -1.74294 | -3.00201 | 102.5262 | 4.27 | -2.70 | 30 |
| 0.11174 | -1.74081 | -3.00990 | 105.0309 | 4.50 | -2.01 | 31 |
| 0.11552 | -1.73917 | -3.02033 | 107.5260 | 5.07 | -1.56 | 32 |
| 0.11931 | -1.73866 | -3.03329 | 110.0283 | 4.67 | -1.32 | 33 |

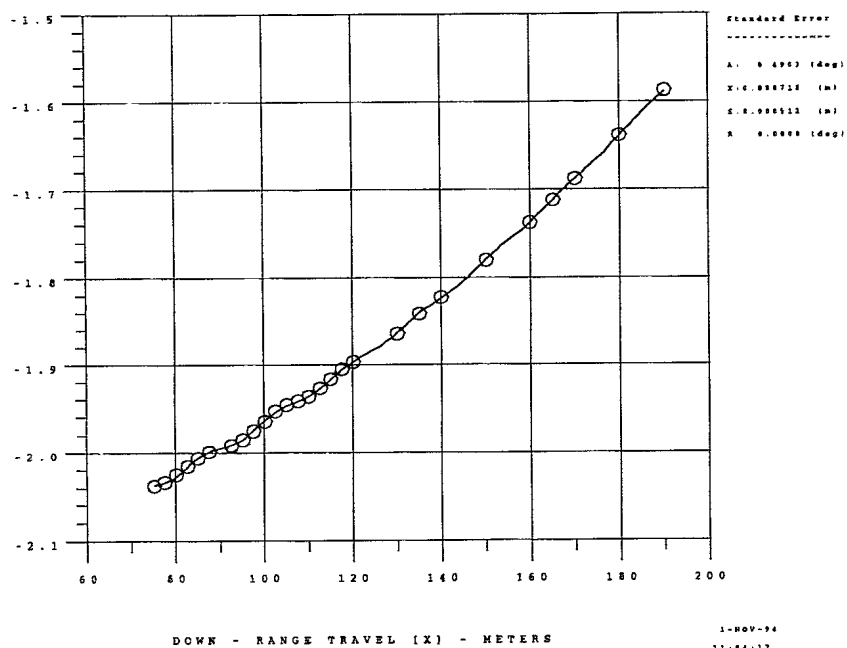UNCLASSIFIED
C.1
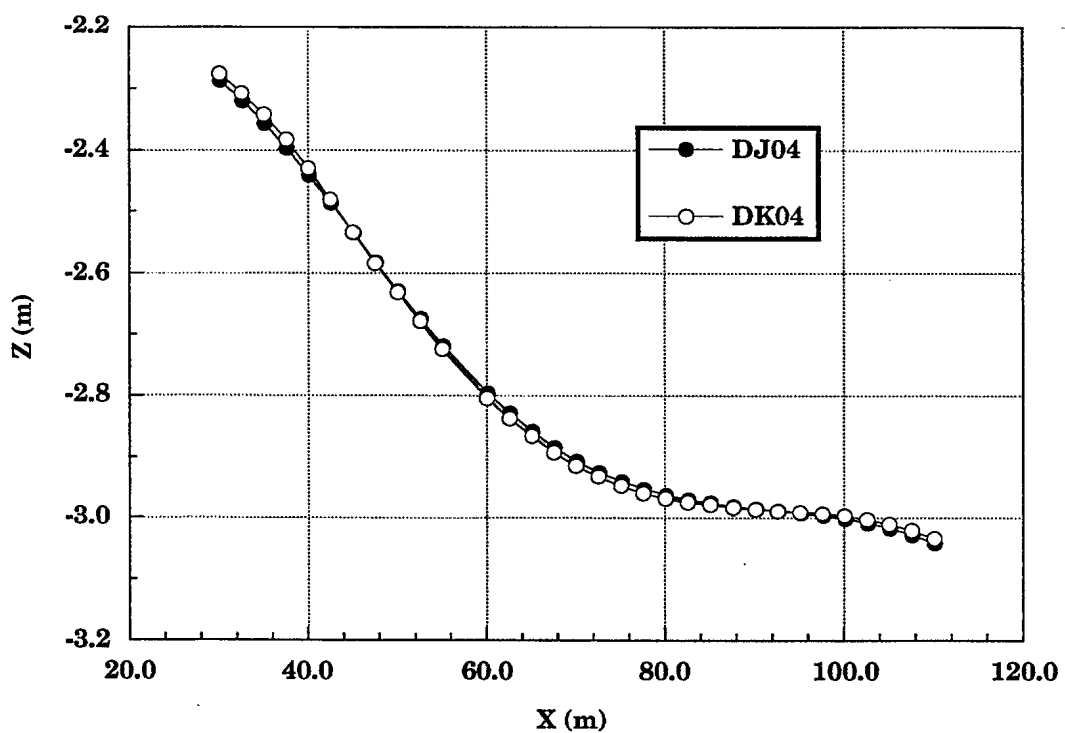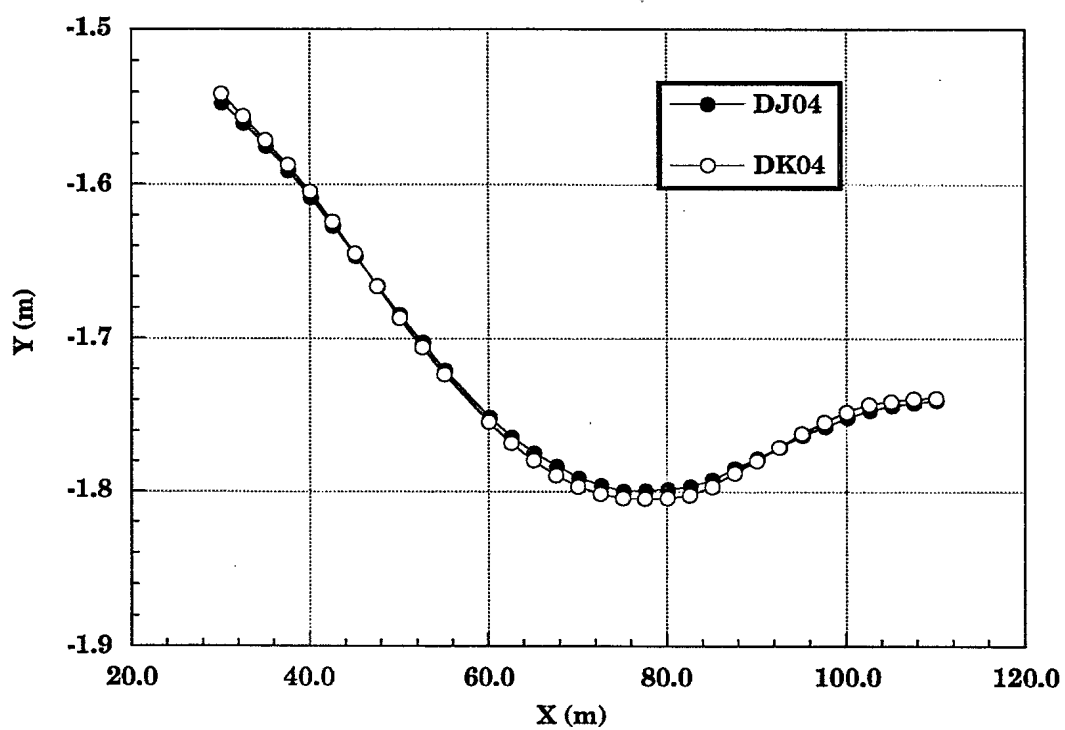
UNCLASSIFIED
C.2
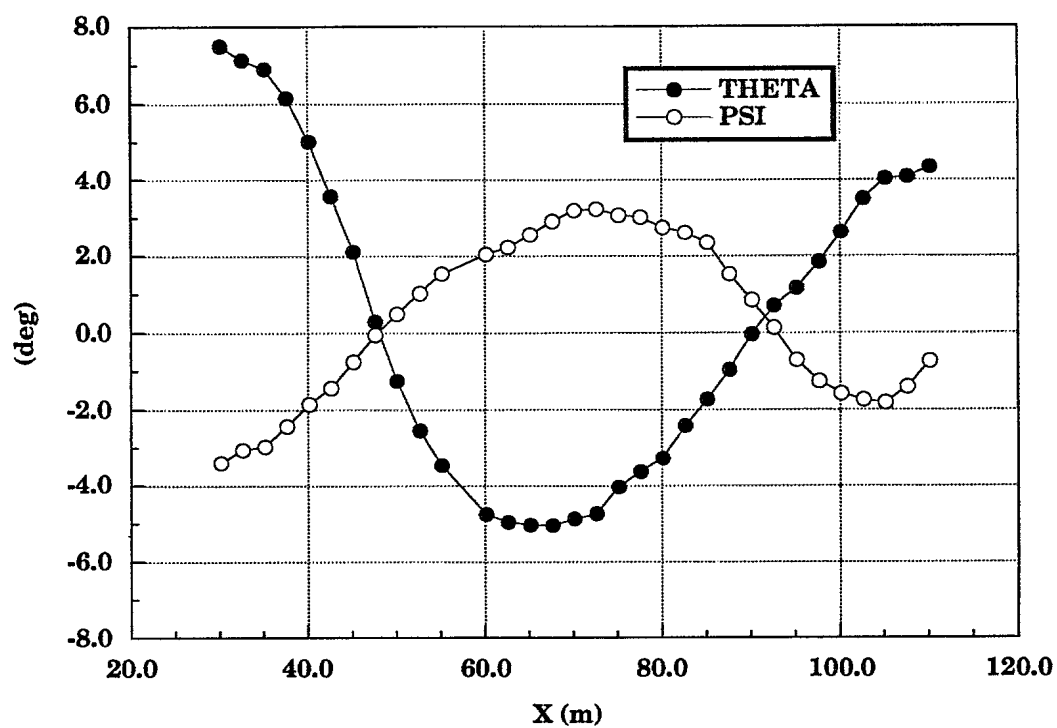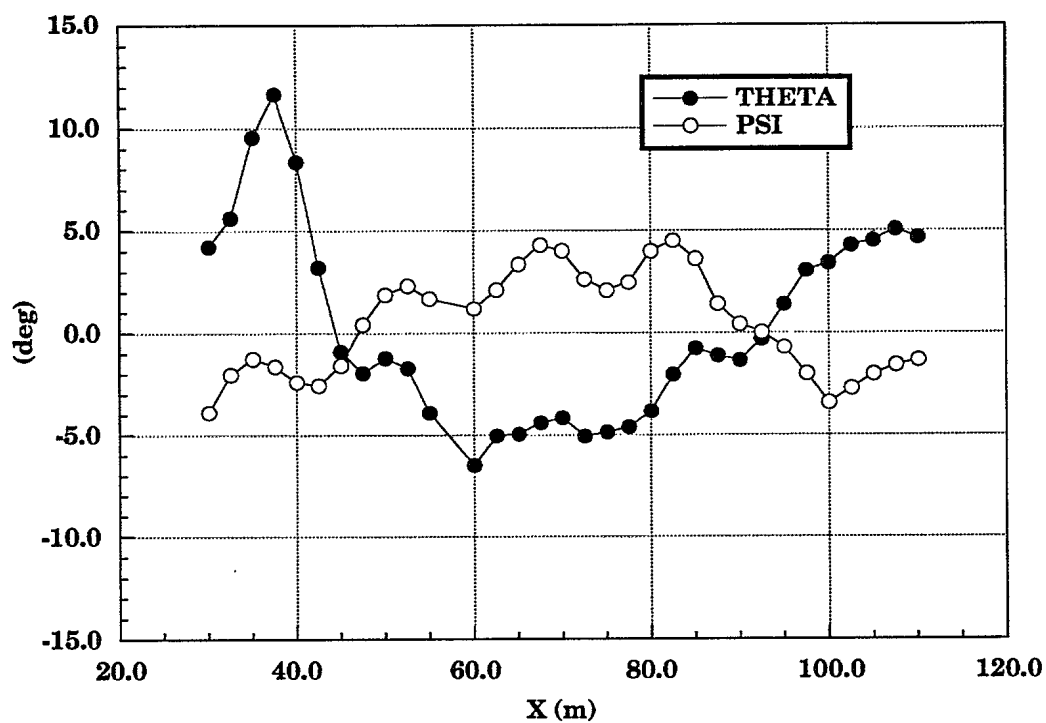
ANNEX D

Motion Plots for Shot DK93051303

# UNCLASSIFIED
## D.1

DK93051303   4-OCT-94   11:55:51      DREV TANDEM (DEUX IEME PRO
6 DOF Reduction - Motion Plots

DOWN - RANGE TRAVEL [X] - METERS

DK93051303   4-OCT-94   11:55:51      DREV TANDEM (DEUX IEME PRO
6 DOF Reduction - Motion Plots

DOWN - RANGE TRAVEL [X] - METERS

# UNCLASSIFIED
## D.2

DK93051303   4-OCT-94   11:55:51      DREV TANDEM (DEUX IEME PRO

6 DOF Reduction - Motion Plots

Standard Error
---------------

A:  0.4953 (deg)
X:0.000719  (m)
E:0.000512  (m)
R:  0.0000 (deg)

**HORIZONTAL MOTION - Y - METERS**

**DOWN - RANGE TRAVEL [X] - METERS**

1-NOV-94
11:03:53

DK93051303   4-OCT-94   11:55:51      DREV TANDEM (DEUX IEME PRO

6 DOF Reduction - Motion Plots

Standard Error
---------------

A:  0.4953 (deg)
X:0.000719  (m)
E:0.000512  (m)
R  0.0000 (deg)
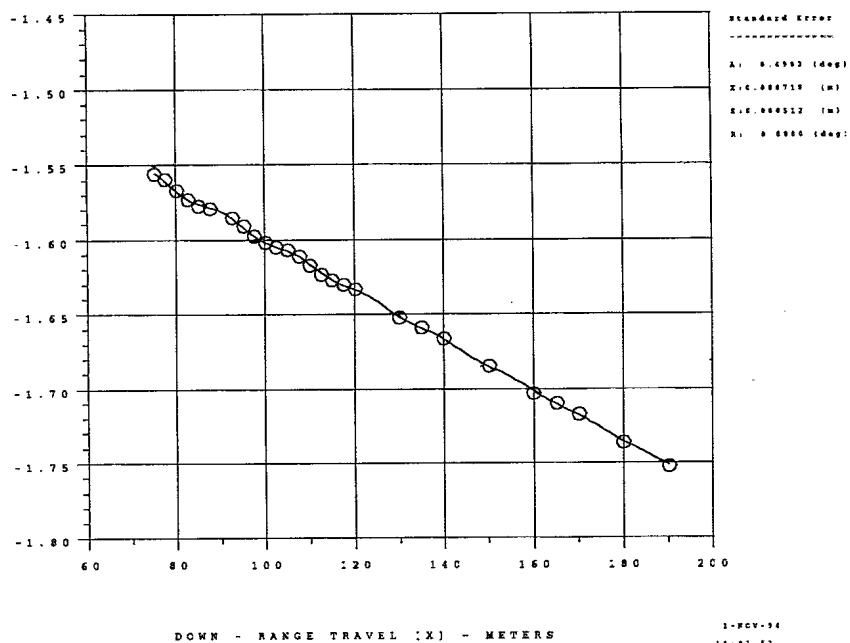
**VERTICAL MOTION - Z - METERS**

**DOWN - RANGE TRAVEL [X] - METERS**
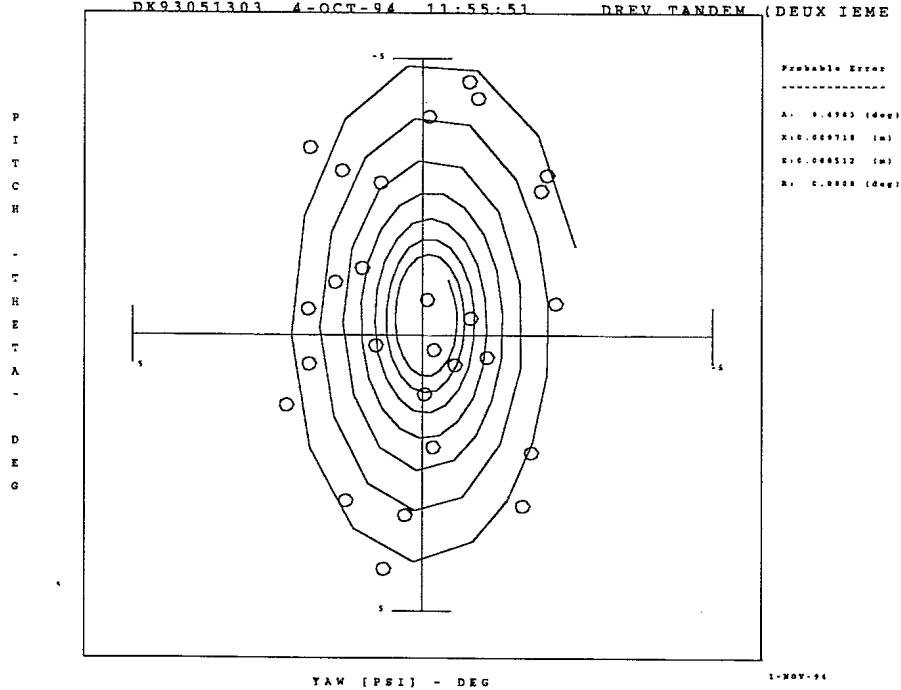
1-NOV-94
11:04:12

UNCLASSIFIED
D.3

DK93051303    4-OCT-94    11:55:51        DREV TANDEM (DEUX IEME PRO

6 DOF Reduction - Motion Plot



DK93051303    4-OCT-94    11:55:51        DREV TANDEM (DEUX IEME PRO



YAW [PSI] - DEG
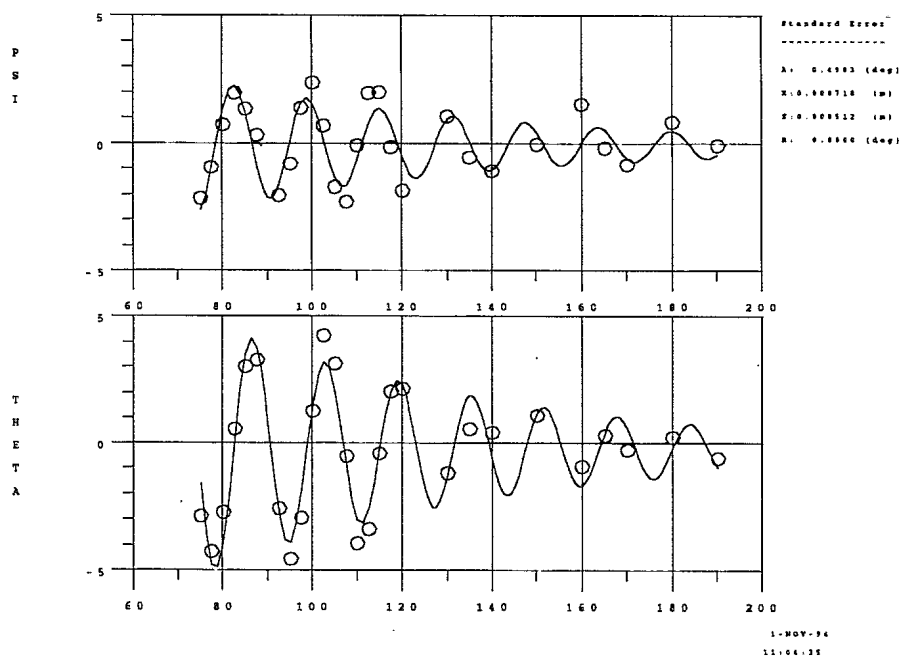
UNCLASSIFIED

<u>INTERNAL DISTRIBUTION</u>

<u>DREV- TM- 9441</u>

1 - Deputy Chief

1 - Director Armaments Division

1 - Director Energetic Material Division

6 - Document Library

1 - A. Dupuis (author)

1 - M. Normand (author)

1 - F. Lesage

1 - B. Girard

1 - E. Fournier

1 - A. Jeffrey

1 - J.-P. Cayouette

1 - G. Dumas

1 - R. Delagrave

1 - G. Bérubé

1 - M. Lauzon

1 - C. Bradette

1 - D. Brousseau

1 - D. Lebel

1 - M. Fortier (Armt)

1 - Maj. M. Bonnet

UNCLASSIFIED

## EXTERNAL DISTRIBUTION

### DREV - TM - 9441

2 - DSIS
1 - CRAD
1 - DRDL
1 - DLR
1 - DAR
1 - DMR
1 - DRDA
1 - DRDM
1 - DFTEM
1 - DACME
1 - DRES
1 - PMO LAV

1 - Mr. W. Hathaway
   Arrow Tech Associates, Inc.
   1233 Shelbourne Road
   S. Burlington, VT 050403
   USA

1 - Dr. B. J. Walker
   AMSMI-RD-SS-AT
   Commander
   U. S. Army Missile Command
   Redstone Arsenal, AL
   35898-5252
   USA

UNCLASSIFIED

1 - Mr. G. L. Winchenbach
1 - Mr. G. Abate
Weapon Flight Mechanics Division
Wright Laboratory Armament Directorate
Eglin AFB, FLA 32542-5434 (USA)

1 - Dr. P. Plostins
1 - Mr. J. M. Garner
1 - Dr. J. Sahu
SLCBR-LF-F
Army Research Laboratory
Aberdeen Proving Ground
Maryland 21005-5066
USA

3 - Drs. C. Berner, M. Giraud and H. F. Lehr
Institut Franco-Allemand de Recherches
5, rue du Général Cassagnou
B.P. 34
68301 - Saint-Louis (France)

3 - Mr. J. Lutes
Mr. A. Bernier
Dr. N. D'Souza
Les Technologies Industrielles SNC Inc.
Usine Le Gardeur
5, montée des Arsenaux
Le Gardeur, Québec
J5Z 2P4

2 - Bristol Aerospace Limited
P. O. Box 874
Winnipeg, Manitoba
R3C 2S4

UNCLASSIFIED

1 - Dr. L. Chan
High Speed Aerodynamic Laboratory
Institute for Aerospace Research
National Research Council Canada
Montreal Road
Ottawa, Ontario
K1A 0R6

1 - Drs. J. Edwards
DRA Military Division
Fort Halstead
Sevenoaks
Kent TN14 7BP
England

1 - Mr. A. J. Sadler
Head AP6
Weapons Aerodynamics Division
DRA
Bedford MK41 6AE
England

1 - Dr. A. R. Rye
DSTO
Surveillance Research Laboratory
P. O. Box 1500
Salisbury, SA 5108
Australia

1 - Mr. C. Ober
Department of Mechanical Engineering
The University of Texas at Austin
Austin, Texas 78759-5329
USA

UNCLASSIFIED

1 - Dr. W. Reinecke
Institute for Advanced Technology
The University of Texas at Austin
4030-2 W. Braker Ln
Austin, Texas 78759-5329
USA

## DOCUMENT CONTROL DATA
(Security classification of title, body of abstract and indexing annotation must be entered when the overall document is classified)

| 1. ORIGINATOR (the name and address of the organization preparing the document. Organizations for whom the document was prepared, e.g. Establishment sponsoring a contractor's report, or tasking agency, are entered in section 8.)<br><br>DEFENCE RESEARCH ESTABLISHMENT VALCARTIER (DREV) | 2. SECURITY CLASSIFICATION (overall security classification of the document. Including special warning terms if applicable)<br><br>Unclassified |
|---|---|

**3. TITLE** (the complete document title as indicated on the title page. Its classification should be indicated by the appropriate abbreviation (S,C,R or U) in parentheses after the title.)

SABOT DESIGN, FREE-FLIGHT TESTS AND ANALYSIS OF A TANDEM PROJECTILE CONFIGURATION AT MACH 2

**4. AUTHORS** (Last name, first name, middle initial. If military, show rank, e.g. Doe, Maj. John E.)

Dupuis, Alain, Normand, Marcel

| 5. DATE OF PUBLICATION (month and year of publication of document)<br><br>February 1995 | 6a. NO. OF PAGES (total containing information. Include Annexes, Appendices, etc.)<br><br>72 | 6b. NO. OF REFS (total cited in document)<br><br>22 |
|---|---|---|

**7. DESCRIPTIVE NOTES** (the category of the document, e.g. technical report, technical note or memorandum. If appropriate, enter the type of report, e.g. interim, progress, summary, annual or final. Give the inclusive dates when a specific reporting period is covered.)

MEMORANDUM

**8. SPONSORING ACTIVITY** (the name of the department project office or laboratory sponsoring the research and development. Include the address.)

DREV

| 9a. PROJECT OR GRANT NO. (if appropriate, the applicable research and development project or grant number under which the document was written. Please specify whether project or grant)<br>PSC 31D | 9b. CONTRACT NO. (if appropriate, the applicable number under which the document was written) |
|---|---|
| 10a. ORIGINATOR'S DOCUMENT NUMBER (the official document number by which the document is identified by the originating activity. This number must be unique to this document.)<br>TM- 9441 | 10b. OTHER DOCUMENT NOS. (Any other numbers which may be assigned this document either by the originator or by the sponsor) |

**11. DOCUMENT AVAILABILITY** (any limitations on further dissemination of the document, other than those imposed by security classification)

- (X) Unlimited distribution
- ( ) Distribution limited to defence departments and defence contractors; further distribution only as approved
- ( ) Distribution limited to defence departments and Canadian defence contractors; further distribution only as approved
- ( ) Distribution limited to government departments and agencies; further distribution only as approved
- ( ) Distribution limited to defence departments; further distribution only as approved
- ( ) Other (please specify):

**12. DOCUMENT ANNOUNCEMENT** (any limitation to the bibliographic announcement of this document. This will normally correspond to the Document Availability (11). However, where further distribution (beyond the audience specified in 11) is possible, a wider announcement audience may be selected.)

FULL UNLIMITED ANNOUNCEMENT

**SECURITY CLASSIFICATION OF FORM**

13. ABSTRACT (a brief and factual summary of the document. It may also appear elsewhere in the body of the document itself. It is highly desirable that the abstract of classified documents be unclassified. Each paragraph of the abstract shall begin with an indication of the security classification of the information in the paragraph (unless the document itself is unclassified) represented as (S), (C), (R), or (U).
It is not necessary to include here abstracts in both official languages unless the text is bilingual).

A series of free-flight tests were conducted at Mach 2 to verify a sabot design that was used to launch a tandem projectile configuration, of similar profile and size, from a 110 mm smooth bore. The projectiles consisted of a four-fin cone-cylinder model with a length-to-diameter ratio l/d of 6 . Four shots were fired, two at an open range to test the sabot functioning and model-sabot integrity at launch, and two in the DREV aeroballistic range to obtain detailed trajectories of the projectiles to study aerodynamic interference effects. The sabot separation process, the measured trajectories, including the separation aspects of the trailing projectile relative to the leading one, are analyzed and discussed. The stability of the models and their aerodynamic characteristic are compared relative to each other and with the results of a same configuration fired individually. Detailed flow photographs showing the complex shock wave structure and their interference on both models flying in close proximity are also given.

14. KEYWORDS, DESCRIPTORS or IDENTIFIERS (technically meaningful terms or short phrases that characterize a document and could be helpful in cataloguing the document. They should be selected so that no security classification is required. Identifiers, such as equipment model designation, trade name, military project code name, geographic location may also be included. If possible keywords should be selected from a published thesaurus. e.g. Thesaurus of Engineering and Scientific Terms (TEST) and that thesaurus-identified. If it is not possible to select indexing terms which are Unclassified, the classification of each should be indicated as with the title.)

SABOT DESIGH
TANDEM PROJECTILES
FREE-FLIGHT TESTS
AEROBALLISTIC RANGE
STABILITY
SHADOWGRAPH
SCHLIEREN
RADAR
SMOOTH BORE  GUN
SIX DEGREE OF FREEDOM
SEPARATION
SUPERSONIC
OPEN RANGE
FINNED PROJECTILE
AERODYNAMIC COEFFICIENTS
INTERFERENCE EFFECTS
FLIGHT DYNAMICS
DYNAMIC STABILITY
MACH 2
TETHERED PROJECTILE
TRAJECTORIES

UNCLASSIFIED

**SECURITY CLASSIFICATION OF FORM**

Requests for documents
should be sent to:


DIRECTOR SCIENTIFIC INFORMATION SERVICES
Dept. of National Defence
Ottawa, Ontario
K1A 0K2
Tel: (613) 995-2971
Fax: (613) 996-0392 .


Toute demande de document
doit être adressée à:


DIRECTEUR - SERVICES D'INFORMATION SCIENTIFIQUE
Ministère de la Défense nationale
Ottawa, Ontario
K1A 0K2

Téléphone:   (613) 995-2971
Télécopieur: (613) 996-0392